Water Adsorption in MOFs

Structures and Applications

Zhang, Bo; Zhu, Zerui; Wang, Xuerui; Liu, Xinlei; Kapteijn, Freek

DOI
10.1002/adfm.202304788

Publication date
2023

Document Version
Final published version

Published in
Advanced Functional Materials

Optimizing Interface Conductivity in Electronics

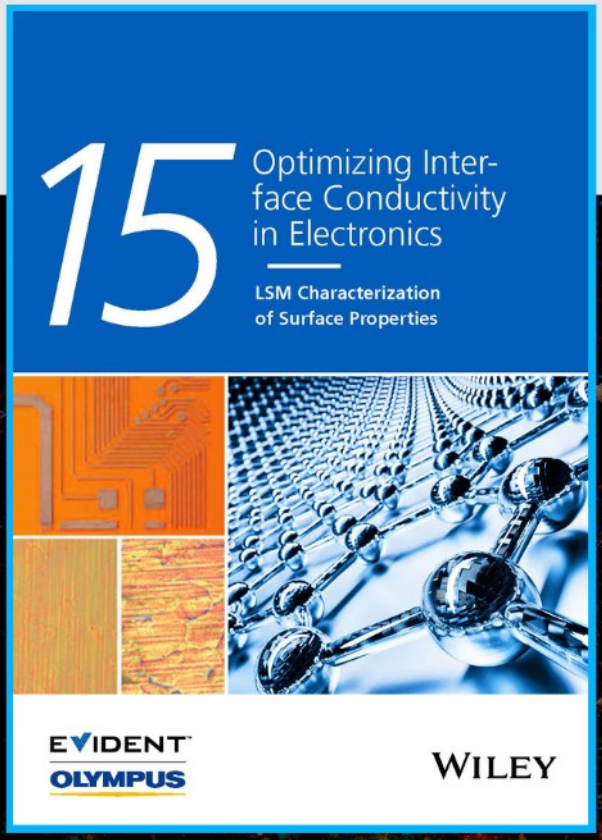

The latest eBook from Advanced Optical Metrology. Download for free.

Surface roughness is a key parameter for judging the performance of a given material's surface quality for its electronic application. A powerful tool to measure surface roughness is 3D laser scanning confocal microscopy (LSM), which will allow you to assess roughness and compare production and finishing methods, and improve these methods based on mathematical models.

Focus on creating high-conductivity electronic devices with minimal power loss using laser scanning microscopy is an effective tool to discern a variety of roughness parameters.

EVIDENT
OLYMPUS

WILEY

ADVANCED FUNCTIONAL MATERIALS
www.afm-journal.de

Water Adsorption in MOFs: Structures and Applications

*Bo Zhang, Zerui Zhu, Xuerui Wang, Xinlei Liu, and Freek Kapteijn**

Metal–organic frameworks (MOFs) are superior sorbents for water adsorption-based applications. The unique step-like water isotherm at a MOF-specific relative pressure allows easy loading and regeneration over a small range of temperature and pressure conditions. With good hydrothermal stability and cyclic durability, it stands out over classical sorbents used in applications for humidity control, water harvesting, and adsorption-based heating and cooling. These are easily regenerated at moderate temperatures using "waste" heat or solar heating. The isotherm thermodynamics and adsorption mechanisms are described, and the presence of MOFs in the water–air system is explained. Based on six selection criteria ≈40 reported MOFs and one COF are identified for potential application. Trends and approaches in further synthesis optimization and production scale-up are highlighted. No-MOF-fits-all, each MOF has its own specific step location matching only with a certain application type. Most applications are technically feasible and demonstrated on the bench-scale or small pilot. Their maturity is benchmarked by their technology readiness level. Retrofitting existing applications with MOFs replacing classical desiccants may lead to rapid demonstration. Studies on techno-economic analysis and life cycle analysis are required for a rational evaluation of the feasibility of promising applications.

1. Introduction

The phase transition that water undergoes by adsorption on or desorption from porous materials and the associated enthalpy change can be utilized in various processes comprising storage or harvesting of water and/or energy, like adsorptive heating and cooling, air conditioning, desalination, drying, etc.

The water-sorbent interaction determines the -conditions dependent- equilibrium loading, the adsorption isotherm, and the enthalpy change, often loading dependent. The sorbent capacity is determined by its specific pore volume. The water isotherms of classical meso- and microporous materials, including silica, alumina, carbon, and zeolites, could be conveniently ordered by the IUPAC physisorption classification over the whole range of hydrophobic to hydrophilic materials[1] until the advent of a completely new class of porous, crystalline hybrid organic–inorganic materials, the metal–organic frameworks (MOFs), and more general porous coordination polymers (PCPs),[2,3] showing structural flexibility and adsorption steps. Regarding water adsorption some of these MOFs exhibited a peculiar step-like isotherm at a certain relative vapor pressure p/p_0, often expressed as % relative humidity, % RH (**Figure 1** left). Depending on the MOF and temperature this step occurs at a different RH, can be less steep but still distinct, is fully reversible, or exhibits desorption hysteresis. The highly porous MOF structure provides water capacities ranging from 0.3 up to 2 g g_{MOF}^{-1}. The observed heat of adsorption for these MOFs is generally 5–15 kJ mol^{-1} higher than the water condensation heat

B. Zhang, X. Liu
Chemical Engineering Research Center
School of Chemical Engineering and Technology
Tianjin Key Laboratory of Membrane Science and Desalination Technology
State Key Laboratory of Chemical Engineering
Haihe Laboratory of Sustainable Chemical Transformations
Tianjin University
Tianjin 300072, China

Z. Zhu, X. Wang
State Key Laboratory of Materials-Oriented Chemical Engineering
College of Chemical Engineering
Nanjing Tech University
Nanjing 211816, China

F. Kapteijn
Catalysis Engineering
Chemical Engineering Dept.
Delft University of Technology
Van der Maasweg 9, Delft 2629 HZ, The Netherlands
E-mail: F.Kapteijn@tudelft.nl

The ORCID identification number(s) for the author(s) of this article can be found under https://doi.org/10.1002/adfm.202304788

DOI: 10.1002/adfm.202304788

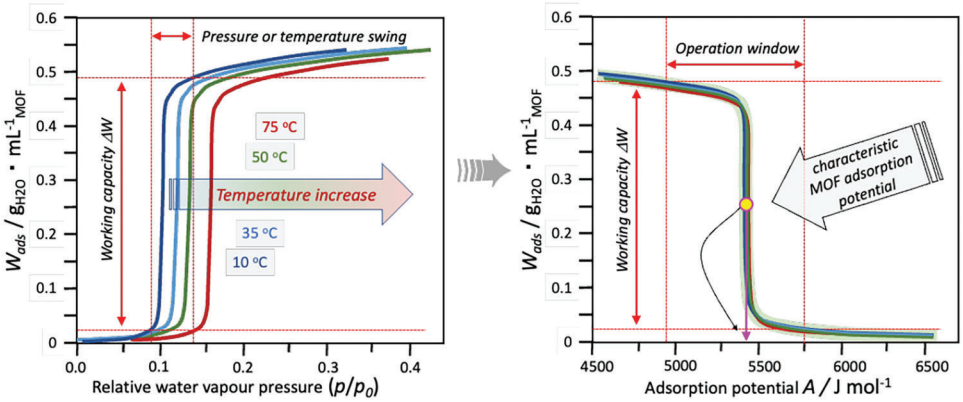

Figure 1. Characteristic example of stepwise water adsorption isotherms on a MOF. Water uptake as a function of the relative water vapor pressure at different temperatures (left), and as a function of the adsorption potential after variable transformation (right). Most MOFs exhibit some uptake before and after the step. Uptake given per unit volume of MOF. Reproduced with permission.[5] Copyright 2020, American Chemical Society.

(vide infra, ≈44 kJ mol^{-1} at room temperature), but lower than classical sorbents as zeolites, and with some exceptions, fairly constant over the loading range of the step.[4]

These peculiar adsorption properties of this type of MOFs, comprising 1) the step-like water uptake at vapor pressures far below condensation, 2) a good working capacity, 3) little or no desorption hysteresis, and 4) a constant heat of adsorption ≈20–30% higher than the heat of condensation, makes them superior over classical materials and highly interesting for applications where water gas–liquid phase transition, vapor pressure control, and energy utilization play a role. Unlike classical sorbents, only a small change in temperature or vapor pressure is needed to load or unload the MOF simultaneously accompanied by a rapid heating or cooling effect, respectively.[5,6]

This opens the attractive utilization of heat sources at temperature levels much below 100 °C for regeneration, like renewable (solar) heat and "waste heat", reducing consumption of primary heat sources and CO_2 emission, and leading to sustainable solutions.

So, the rapid increase in water adsorption studies on MOFs and related materials exploring the MOF–water interaction in all kinds of applications is not surprising.

This review in Advanced Functional Materials builds further on our previous reviews on heat reallocation and humidity control,[5,6] extending on recent literature with emphasis on new MOF materials, synthesis approaches, and selected applications with a focus on open systems. Before describing the various applications, some basic elements are (re)introduced for a proper understanding of the phenomena involved and essential engineering aspects to consider in the presented applications. This paper concludes with an outlook on future expectations, needs, and challenges.

2. Aspects of Water Adsorption in MOFs

2.1. Isotherm Properties, Thermodynamics

The water adsorption isotherm is dependent on both the relative pressure and the temperature. Following Dubinin and Polanyi these independent variables can be combined into one, the Polanyi adsorption potential $A(p/p_0,T)$, which is the molar Gibbs free energy of adsorption with opposite sign, resulting in:

$$W\left(\frac{p}{p_0},T\right) \Rightarrow W(A) = W_{max}\exp\left[-\left(\frac{A}{E}\right)^n\right] \qquad A = -RT\ln\left(\frac{p}{p_0}\right) \tag{1}$$

Now all isotherms of a MOF sorbent at different conditions collapse onto one single characteristic curve with a step located at the MOF-specific characteristic adsorption energy E (Figure 1 right).[6] For a less steep isotherm the inflection point α (= p/p_0) in the step is taken as reference.

2.2. Operation and Psychrometric Chart

Water adsorption-based applications all feature two coupled cyclic operated units, one being a MOF–water contactor, and the other a water processing unit. In the contactor water adsorption or release occurs, while releasing adsorptive heat to or absorbing regeneration heat from the environment, respectively. In the processing unit water is condensed or evaporated with the respective associated heat removal or supply.

In "closed" systems only exchange of heat takes place, and the amount of system water is fixed, whereas in "open" systems also water supply and removal take place. **Figure 2** shows both cases schematically.[5] In the detailed way of coupling the units, cyclic operation modes, and conditions the different applications distinguish themselves. In water harvesting capacity and productivity are important targets, while in heat reallocation energy storage density and productivity (specific heating or cooling power) are aimed for. The analysis of closed systems is based on the Clausius-Clapeyron diagram,[6–8] while that for open systems is the psychrometric chart for the water-air component mixture.[9] With the focus on open systems in this manuscript, the latter is extended with the use of MOFs.

The operation in both subunits depends on the vapor–liquid and vapor–sorbent interaction, depending on temperature and water vapor pressure. Based on the Gibbs phase rule, stating that three degrees of freedom (i.e., intensive variables such as temperature, pressure, composition) define completely a single phase

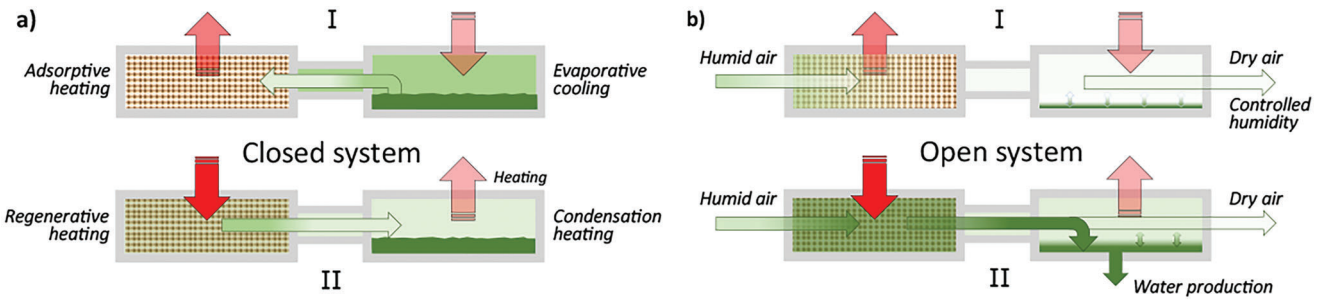

Figure 2. Schematic configuration of a) a "closed" and b) an "open" application in adsorption (I) and regeneration (II) mode. Key: Red arrows, energy flow, green arrows water flow direction. Color intensities suggest temperature and concentration levels. Reproduced with permission.[5] Copyright 2020, American Chemical Society.

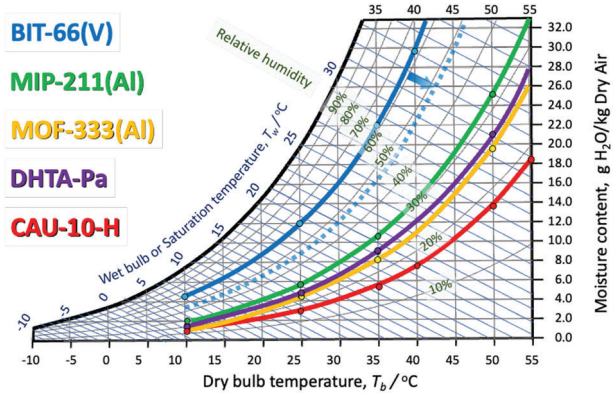

Figure 3. Psychrometric chart of the water/air system at 1 atm. Included in color the loci of conditions at which selected sorbents exhibit their water uptake step. The dashed curve exemplifies the desorption hysteresis shift for BIT-66(V). Chart drawn based on literature data refs. [4,10–13].

two-component system (air–water vapor). Hence, all relevant intrinsic properties can be represented in a two-dimensional graph for atmospheric pressure, the psychrometric chart.[9] **Figure 3** shows the moisture content or absolute humidity AH (g_{H2O} $kg_{dry\ air}{}^{-1}$) as a function of the ("dry bulb") temperature of the air–water vapor mixture. The degrees of freedom reduces by one when liquid water is also present in equilibrium with its saturated vapor (100% RH), indicated by the saturation line. The presence of a MOF sorbent with a steep water uptake step introduces another equilibrium line at lower RH. Using the adsorption potential *A* this is indicated for a few MOFs based on their adsorption isotherm data. This curve runs slightly steeper than the iso-RH lines due to the higher heat of adsorption (vide supra). At conditions above this line, an unsaturated MOF will adsorb water decreasing the AH to the level of this saturation line, while at conditions below this line, water is released from a saturated MOF. So, small changes in humidity and/or temperature can trigger the state of the MOF (loaded or unloaded), and air humidities are controlled without the presence or formation of liquid water. In case a MOF shows adsorption–desorption hysteresis this results in separate curves for both processes since higher temperature or lower humidity is needed in desorption, as indicated for BIT-66(V).[10] The psychrometric chart is the basis for all considerations regarding humidity control in open systems, such as air conditioning, desiccation, desalination, and water harvesting.

2.3. Engineering Aspects

In all applications the simultaneous mass transport of water vapor and, in opposite direction, transport of generated associated heat occurs. In both open and closed-type applications scale independent (adsorption thermodynamics) phenomena have to be combined with scale-dependent (mass and energy transport both on the MOF and device level) phenomena to obtain an optimally balanced system for energetically and productivity-efficient performance.[14] This is where applications differ in specific configurations.[5] The porous structure of MOFs and the small particle size are a downside for thermal conductivity and pressure drop in packed beds, so in formulation using a binder particulate composites,[15–18] coated or co-spun fibers and fabrics[19–22] or thin MOF coatings on heat conducting materials are frequently suggested.[6,23] Stimuli-responsive MOFs provide an alternative to rapid water release by localized heating.[24–29] However, to improve the water transport the (macro)porosity in these composites or coatings is generally increased,[18,19] lowering the MOF loading with an adverse effect on the volumetric capacity of the whole system. The molecular transport in the small pores of the MOFs will be of the Knudsen diffusion type[18] mixed with adsorptive interaction with functional groups in the pore wall, i.e., surface diffusion.

Recently, superfluidity was suggested to play a role in the small micropores where Van der Waals' adsorption potential of the opposite walls overlap, resulting in a kind of levitated molecule that moves without friction[30] as in carbon nanotubes.[31] The heterogeneous and corrugated MOF pore walls may render this phenomenon questionable and still needs to be demonstrated.

3. Adsorption Mechanism – Phase Transition

The intriguing steep uptake step of the water adsorption isotherm asks for a more detailed interpretation.

Generally, water adsorption is attributed to several phenomena:

- Specific adsorption at open metal sites, hydroxyls, or other polar (hydrophilic) surface groups, serves as nucleation centers for further water interaction.
- Adsorption through hydrogen bonding at present nucleation centers forms localized water clusters, increasing with increasing relative pressure[32] and filling of micropores.[33]

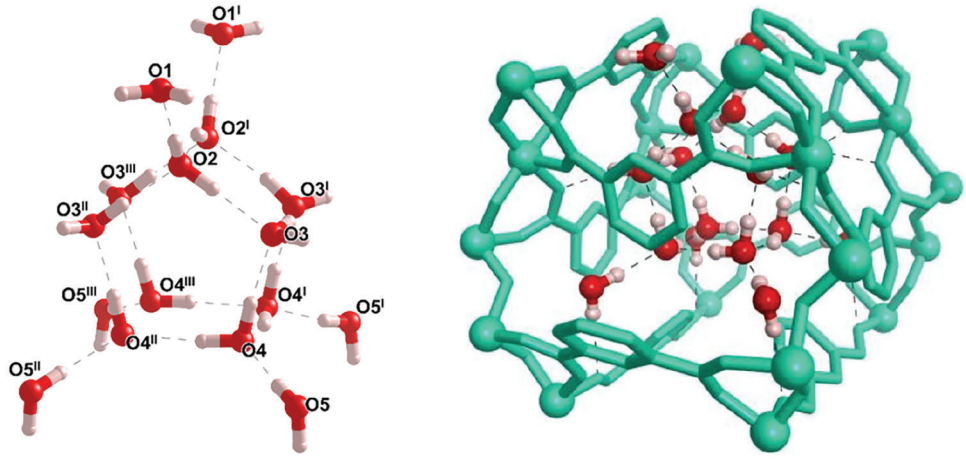

Figure 4. $(H_2O)_{16}$ water cluster (left) in fully hydrated CAU-10(Al)-H cavity (right), The hydrated CAU-10(Al)-H framework with contained water cluster is based on results from single crystal XRD. Reproduced with permission.[38] Copyright 2023, Wiley-VCH.

- Capillary condensation. For water, pores with a diameter larger than a critical diameter of ≈2 nm exhibit capillary condensation after cluster adsorption.[5] Due to the thermodynamic irreversibility of capillary condensation, hysteresis is observed between the adsorption and desorption branches.[32–34] As an exception to the rule a hysteresis has also been observed for some microporous materials. Functionalized carbons and one MOF, Cr-soc-MOF-1, show hysteretic behavior attributed to the formation and relaxation of superclusters of water upon adsorption and desorption.[35,36]
- Phase transition. An arrangement of water vapor molecules into a regular solid-like cluster structure (deposition) above a specific vapor pressure, and their release below this pressure (sublimation) without any hysteresis. Diffraction studies showed this initially for CAU-10(Al)-H[13] and MOF-801[37] (vide infra[4,38]). This is completely analogous to the vapor–liquid phase transition (condensation) of pure water, but now at a much lower vapor pressure. In most cases, this step uptake is preceded by some leading water uptake (nucleation) at hydrophilic sites. This is not a necessary condition for the step, as the highly hydrophobic COF-432 shows with its cylindrical pores of 0.75 nm.[39] Apparently, in this case, the cluster and pore size match nicely, inducing cluster formation.
- Sorption-induced structural changes may affect the uptake behavior.[33,40] Functionalization of the MIL-53(Al) linker changes its flexibility. The MIL-53(Al)OH expands from the narrow pore to the large pore structure doubling its water uptake at higher RH, which results in a large desorption hysteresis as well.[33,41] Co_2Cl_2(BTDD) possesses 1D mesoporous (2.2 nm) channels, but its pore size decreases slightly below 2 nm after the initial water adsorption on the open metal sites, and capillary condensation and the associated hysteresis does not occur.[42]

Many of the MOFs that exhibit a steep step without hysteresis have a 1D pore structure with pores of ≈0.7 nm. The water adsorption heat of CAU-10(Al)-H (53.5 kJ mol^{-1}) is higher than the heat of water condensation (44.0 kJ mol^{-1} @298 K) and the entropy is lower than in liquid water, 58 versus 70 J mol^{-1} K^{-1}. This suggests a regular and immobile state. Similar heats of adsorption (50.4–52.8 kJ mol^{-1}) are reported for a series of multivariate MOFs synthesized by varying the relative linker amounts from MOF-303 to MOF-333.[4] The isosteric heat of water adsorption of DHTA-Pa equals ≈50 kJ mol^{-1} for the step uptake loading and drops to the heat of condensation of ≈44 kJ mol^{-1} for the gradual water uptake after the step, elegantly showing a distinct difference between the water–wall interaction and the water–water interaction.[12] The water structure in CAU-10(Al)-H and -CH_3 is analyzed in detail by Van der Veen et al.[38] by single crystal XRD revealing $(H_2O)_{14}$ clusters in the former upon completing the uptake step, while at higher relative pressures a further water uptake results in the addition of two more molecules to $(H_2O)_{16}$ clusters in the 1D channel of CAU-10(Al)-H (**Figure 4**). Similarly, the presence of $(H_2O)_{19}$ clusters could be demonstrated in the cavities of water-loaded MIL-160, while the development of nucleation, clustering, and network formation at various loadings in MOF-303 was unveiled by Hanikel et al.[4]

The more hydrophobic CAU-10(Al)-CH_3 impedes the water adsorption at hydrophilic sites and introduces steric hindrance leading to weaker and smaller cluster formation. Based on their own results and literature analysis the authors conclude that for a steep water adsorption isotherm cluster formation is required, equivalent to a phase transition,[5] and each MOF exhibits different cluster structures.[4,38,43] Moderate hydrophilic sites induce the onset of the step in a framework still consisting mostly of hydrophobic pore walls. The pore geometry should allow accommodation of energetically favorable water cluster(s). In a series of multivariate linker MOFs it is elegantly shown that the reduction in polarity decreases the step steepness while shifting its inflection point to higher relative pressures.[4]

The large variation of the location of the p/p_0 step value (a) for different MOFs indicates that the energetics of the formed water clusters are quite different, showing the importance of pore wall geometry and polarity, and not only size, although a wider pore will shift the step to higher relative pressure due to the relative increase of water–water interactions over water–wall interactions.[34,44]

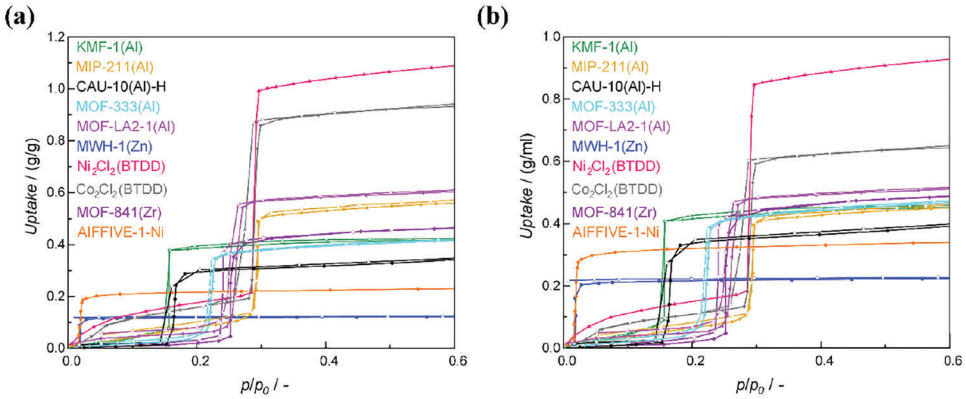

Figure 5. Water adsorption (solid symbols) and desorption (open symbols) isotherms, presented in a) gravimetric and b) volumetric uptake, of selected MOFs, which have very steep uptake at inflection points at 298 K: KMF-1(Al) (@313 K),[54] MIP-211(Al),[71] CAU-10(Al)-H,[13] MOF-333(Al),[4] MOF-LA2-1(Al),[55] MWH-1(Zn) (@293 K),[56] Ni_2Cl_2(BTDD),[48] Co_2Cl_2(BTDD),[42] MOF-841(Zr),[37] AlFFIVE-1-Ni (@308 K).[57] The crystal density of MOFs is taken from Table 1. Lines are shown to guide the eye. The full relative pressure range is given in SI.

4. State-of-the-Art MOFs

4.1. MOF Synthesis for Water Sorption Applications

With the in-depth development, increasingly more MOFs have shown water adsorption capacity characteristics. Six selection criteria have been summarized by Liu et al.[5] to decide whether a MOF is fit for water adsorption-based applications, comprising:

(a) Good hydrothermal stability. For water-related applications, MOF will inevitably contact with water (liquid or vapor state), so its stability is of utmost importance. The hydrothermal stability of MOF was discussed in detail in these reviews.[5,6,41]

(b) A steep uptake isotherm at a specific relative pressure. MOFs with step-shaped isotherms, which allow adsorption/desorption of substantial amounts of water with only minor swings in pressure and/or temperature, are desirable for practical applications. Samples are collected and exemplified in **Figure 5**.

(c) A large water working capacity, i.e., the reversible uptake/release per unit of MOF under working conditions. A greater water working capacity means higher efficiency during a working cycle.

(d) Make full use of adsorption–desorption hysteresis, if present. Different applications have different requirements for the desorption properties of MOFs. For atmospheric water harvesting, MOF with minimal or no hysteresis in desorption is desired. On the contrary, a specific hysteresis in desorption is needed for indoor humidity control (vide infra).

(e) High cycling durability. The high cycling durability of MOF is an important factor affecting the application stability. The performance degradation of MOF due to repeated adsorption and desorption of water is unacceptable.

(f) Facile adsorption–desorption, fast mass, and heat transport kinetics for the desired energy efficiency.[5] Only those MOFs, which can achieve efficient adsorption/desorption in a short time with high thermal diffusivity, are the best candidates for application,[12] although it is noted that the implementation is at least as important.

As shown in **Table 1**, 42 types of MOFs and 1 type of COF have been selected based on the above criteria. The structure and water sorption properties of these MOFs are studied below. Firstly, direct-synthetic MOFs classified into mesoporous (2–50 nm pore diameter) and microporous (< 2 nm pore diameter) ones are discussed. Then, post-synthetic MOFs and related strategies for adjusting their water sorption property are summarized.

4.1.1. Direct Synthesis MOFs

Mesoporous MOFs. Capillary condensation behavior and adsorption–desorption hysteresis often take place. MIL-101(Cr)[45] has two types of mesoporous cages with internal free diameters of 2.9 and 3.4 nm connected by windows of 1.2 and 1.5 nm and displays a large water capacity (up to 1.73 g g^{-1}) and an inflection point at $\alpha = \approx 0.4$.[5] MIL-100(Fe)[46] with mesoporous cages (2.5 and 2.9 nm) features basically isotherms of similar shape with a lower inflection point ($\alpha = \approx 0.35$) and lower capacity (up to 0.87 g g^{-1}) as MIL-101(Cr).[5] Co_2Cl_2(BTDD)[42] possesses 1D mesoporous (2.2 nm) channels, but its pore size decreases slightly below 2 nm after the initial water adsorption on the open metal sites, thus no capillary condensation occurs.[5] A steep uptake at $p/p_0 = 0.29$ and a high water capacity (up to 0.97 g g^{-1}) are observed (Figure 5). Ni_2Cl_2(BTDD) has a similar structure and isotherm shape as Co_2Cl_2(BTDD) but a higher water capacity (up to 1.14 g g^{-1}).[47,48]

BIT-66(V) possesses 1D hexagonal channels with a maximum dimension of ≈2.58 nm.[10] Two types of pores with diameters of 0.65 and 2.58 nm are distinguished based on nonlocal DFT method.[10] The isotherm of BIT-66(V) at 298 K reveals an initial water uptake below $p/p_0 = 0.55$, which is mainly attributed to the open metal sites and micropores adsorption. A steep uptake with the 0.55 g g^{-1} uptake capacity is observed between $p/p_0 = 0.55$–0.65. Maximum water capacity of 0.71 g g^{-1} is reached at $p/p_0 = 0.98$ and the isotherms have an S-shape with a significant hysteresis loop at $p/p_0 = 0.45$–0.6 between the adsorption–desorption branches (Figure S1, Supporting Information). In durability testing an initial capacity loss (≈12%) is observed during the first 20 cycles, reaching a constant level up to 50 cycles.[10]

Table 1. Structural information and water sorption properties of selected MOFs based on six criteria (see text).

Material	Linker	α [-][a)]	q_{max} [g g^{-1}][b)]	d_{pore} [Å]	Pore space	ρ_c [g mL^{-1}]	$-\Delta_{ads}H$ [kJ mol^{-1}][c)]	V_p [cm^3 g^{-1}][d)]	Stability	Reference
Cr-soc-MOF-1	TCPT	0.69	1.95	17	1-D	0.381	–	2.1	No loss in Δq over 100 ads. Cycles / with significant hysteresis	[35]
LiCl@MIL-101(Cr)	BDC	0.38	1.87	29, 33	3-D	–	–	0.69	No loss in Δq over 20 ads. Cycles	[81]
MIL-101(Cr)	BDC	0.4	1.73	29, 34	3-D	0.48	75–36	–	–	[6,32]
Ni_2Cl_2(BTDD) (Flow reactor scale-up)	BTDD	0.29	1.14	22	1-D	0.852	–	–	–	[48]
NU-1500-Cr	PET	0.49	1.11	14	1-D	0.539	–	1.24	No loss in Δq over 20 ads. Cycles	[59]
ISO-NU-1000(Zr)	TBAPy-2	0.68	1.10	13, 32	1-D	–	–	1.27	No loss in Δq over 22 ads. Cycles / with significant hysteresis	[72]
Facac-NU-1000(Zr)	TBAPy	0.77	1.02	12.7, 27.6	1-D	0.631	–	1.36	No loss in q_{max} over 20 ads. Cycles / with significant hysteresis	[87]
Co_2Cl_2(BTDD)	BTDD	0.29	0.97	22	1-D	0.69	55–41	–	6.3% loss in Δq over 30 ads. Cycles	[42]
NU-913(Zr)-TFA	L3	0.54	0.85	14 × 20	1-D	–	–	0.77	7.4% loss in q_{max} after 10 ads. Cycles / with hysteresis	[76]
MIL-100(Fe)	BTC	0.35	0.79	25, 29	3-D	0.72	65–40	0.82	–	[46]
BIT-66(V)	BTB	0.62	0.71	6.5, 25.8	1-D	–	–	0.87	12% loss in q_{max} after 50 ads. Cycles / with significant hysteresis	[10]
DHTA-Pa[e)]	Pa	0.26	0.71	14	1-D	–	51–44	–	No loss in Δq over 80 ads. Cycles	[12]
MOF-808(Zr)-Br	BTC-Br	0.17	0.70	15.9	3-D	1.199	–	0.67	7.5% loss in q_{max} over 21 ads. Cycles	[74]
UiO-67-4Me-NH_2-38%	Mixed	0.58	0.66	10.8	3-D	–	–	0.69	No loss in Δq over 10 ads. Cycles / with significant hysteresis	[71]
MOF-LA2-1(Al)	PZVDC	0.26	0.64	11	1-D	0.847	65.8–47.3	0.67	No loss in Δq over 150 ads. Cycles	[55]
MOF-808(Zr)$PDS_{1.7}$	BTC/PDS	0.23	0.61	–	3-D	–	–	0.62	20% loss in Δq over 5 ads. Cycles	[75]
MIP-211(Al)	*t,t*-muconate	0.29	0.61	8.5	1-D	0.807	48.6–45.5	0.60	No loss in Δq over 40 ads. Cycles	[11]
MOF-303(Al) (Vessel scale-up)	PZDC	0.14	0.59	6	1-D	–	–	–	–	[88]
MOF-808(Zr)$NDS_{1.8}$	BTC/NDS	0.20	0.53	–	3-D	–	–	0.56	13% loss in Δq over 5 ads. Cycles	[75]
MOF-841(Zr)	MTB	0.22	0.51	13.3	3-D	1.05	58–42	0.53	7% loss in q_{max} after 5 ads. Cycles	[37]
FDM-92(Al)	BPDC	0.33	0.50	12.2	1-D	0.878	–	0.61	10.6% loss in q_{max} over 100 ads. Cycles	[73]
Y-shp-MOF-5	BTEB	0.63	0.48	12	1-D	0.963	–	0.63	9% loss in q_{max} after 1000 ads. Cycles / with significant hysteresis	[58]
Zr-adip	ADIP	0.11	0.48	6.6, 12.8	1-D	1.17	51–46	0.47	No loss in Δq over 300 ads. Cycles	[69]

(*Continued*)

Table 1. (Continued).

Material	Linker	α [-][a]	q_{max} [g g^{-1}][b]	d_{pore} [Å]	Pore space	ρ_c [g mL^{-1}]	$-\Delta_{ads}H$ [kJ mol^{-1}][c]	V_p [cm^3 g^{-1}][d]	Stability	Reference
MOF-303(Al)	PDC	0.13	0.45	6	1-D	1.159	50–40	0.54	No loss in Δq over 150 ads. Cycles	[53]
MIL-125(Ti)-NH_2	NH_2-BDC	0.2	0.45	6, 12	3-D	0.81	–	0.51	–	[34]
Al-fumarate	FA	0.27	0.45	5.7 × 6.0	1-D	1.24	50–42	0.48	No loss in Δq over 4500 ads. Cycles	[89]
MIP-200(Zr)	MDIP	0.18	0.45 (303 K)	6.8, 13	1-D	1.16	70–45	0.40	6% loss in Δq over 1–10 ads. Cycles and no loss in Δq over 10–40 ads. Cycles	[63]
CAU-1(Al)-OH	BDC-OH	0.48	0.45	6.2, 8.6	3-D	–	–	0.78	No loss in Δq over 500 ads. Cycles / with hysteresis	[68]
MOF-333(Al)	FDC	0.22	0.45	9.4	1-D	1.122	52.7–46.8	0.523	–	[4]
KMF-1(Al)	PyDC	0.16	0.43 (313 K)	5.7	1-D	1.08	57–52	0.473	No loss in Δq over 50 ads. Cycles	[54]
CAU-23(Al)	TDC	0.27	0.42	7.6	1-D	1.07	48.2	0.48	No loss in Δq over 5000 ads. Cycles	[52]
Zr-Fum HT	FA	0.10	0.41 (313 K)	5.8, 11.2	3-D	1.59	52–45	0.553	No loss in Δq over 50 ads. Cycles	[86]
MIL-53(Al)-OH	OH-BDC	0.75	0.40	17 × 12	1-D	–	–	–	–	[67]
MIL-160(Al)	FDC	0.09	0.38 (303 K)	5	1-D	1.068	64–43	0.40	No loss in Δq over 10 ads. Cycles	[51]
CAU-10(Al)-H	1,3-BDC	0.16	0.37	7	1-D	1.15	53.5	–	No loss in Δq over 9 ads. Cycles	[13]
UiO-66(Zr)	BDC	0.31	0.37	6, 9, 11	3-D	1.23	–	0.35	No loss in q_{max} over 2 ads. Cycles	[41,60–62]
MOF-801(Zr)	FA	0.09	0.36	4.8, 5.6, 7.4	3-D	1.68	62–47	0.45	Stable over 5 ads. Cycles	[37]
Co-CUK-1	PDC	0.12	0.30 (303 K)	13.4 × 13.0	1-D	1.46	60–45	0.26	No loss in Δq over 50 ads. Cycles	[64]
AlFFIVE-1-Ni	Pyrazine	0.02	0.24 (308 K)	–	1-D	1.48	63	0.102	No loss in Δq over 14 ads. Cycles	[57]
MWH-1(Zn)	BPY/BTEC	0.02	0.13 (293 K)	3.6	2-D	1.839	–	–	–	[56]
Multivariate MOF-303(Al)&CAU-23(Al)	PZDC/TDC	–	–	–	1-D	–	54.2–48.6	–	–	[78]
Multivariate MOF-303(Al)&MOF-333(Al)	PZDC/FDC	–	–	–	1-D	–	52.8–50.4	–	–	[4]
Mixture of CAU-10(Al)-H& Al-fumarate	1,3-BDC/FA	–	–	–	–	–	–	–	–	[79]

[a] Inflection point of water uptake step, the relative pressure for which capacity is 50% of q_{max}; [b] Maximum capacity, measured at 298 K unless otherwise stated; [c] Heat of adsorption (isosteric or average of isosteric heat); [d] Pore volume, from N_2 adsorption at 77 K; [e] DHTA-Pa is a COF.

Microporous MOFs. Cluster adsorption is always present. Al-fumarate[49] features a rigid framework with lozenge-shaped 1D channels (free dimensions of 0.57 nm × 0.60 nm). A steep uptake happens at p/p_0 = 0.2–0.3, and the hysteresis is narrow.[5] CAU-10(Al)-H,[50] built up from helical chains of *cis*-corner shared AlO_6 octahedra, possesses 1D square-shaped, sinusoidal channels with a diameter ≈0.7 nm and shows a desirable S-shaped adsorption isotherm with main loading lift at p/p_0 = 0.16 and no hysteresis (Figure 5).[5,11] MIL-160(Al)[51] is isostructural to CAU-10(Al),[11] featuring square-shaped sinusoidal 1D channels with a diameter ≈0.5 nm.[5] It has a less steep type V isotherm with a low inflection point at p/p_0 = 0.09 without hysteresis.[5] CAU-23(Al),[52] with a sulfur-based linker instead of the furan-based linker in MIL-160(Al) contains chains of mixed cis/trans corner-shared AlO_6 octahedra and has 1D square channels (side length of 0.76 nm). The steep uptake in the isotherm is observed at p/p_0 = 0.27 with little hysteresis.[5] MOF-303(Al),[53] consists of alternating chains of cis- and trans-connected corner-sharing AlO_6 octahedra, featuring 1D hydrophilic channels with a diameter ≈0.6 nm. It displays a less steep type IV isotherm with a low inflection point at p/p_0 = 0.13, and minimal hysteresis,[5] while the isomorphous MOF-333(Al) does possess the steep isotherm with an inflection point at p/p_0 = 0.21. KMF-1(Al),[54] also built up from *cis*-corner shared AlO_6 octahedral chains, possesses 1D square-shaped, sinusoidal channels with a diameter ≈0.57 nm. The S-shaped isotherm with a notable steep uptake and no hysteresis is observed at p/p_0 = 0.16 (Figure 5). A moderate isosteric heat of water adsorption ranging from 52–57 kJ mol^{-1} suggests a facile regeneration of KMF-1(Al).[54] The water uptake remained unaltered over 50 adsorption cycles.[54]

Y-shp-MOF-5[58] possesses triangular 1D channels with an opening of 1.2 nm. A significant hysteresis is observed between the type-IV-like adsorption and desorption isotherms with inflection points at p/p_0 = ≈0.63 and p/p_0 = ≈0.45, respectively.[5] Cr-soc-MOF-1[35] has well-defined 1D infinite channels with a diameter ≈1.7 nm. A significant hysteresis is observed between the S-shaped adsorption and desorption isotherms with inflection points at p/p_0 = ≈0.61 and p/p_0 = ≈0.40, respectively.[5] NU-1500-Cr[59] has uniform hexagonal 1D channels about the size of 1.4 nm. A steep uptake at p/p_0 = 0.49 is observed, and a maximum capacity (up to 1.11 g g^{-1}) is reached at p/p_0 = 0.9 (Figure S1, Supporting Information).[59] No loss in water capacity is found over 20 adsorption cycles.[59]

UiO-66(Zr)[60] has a face-centered cubic lattice (*fcc* topology) with three types of pore sizes of 0.60, 0.90, and 1.1 nm,[61,62] and displays an initial low water uptake till p/p_0 = ≈0.25.[5] UiO-66(Zr) features a small hysteresis loop and outstanding structural stability.[5] MOF-801(Zr),[37] also known as Zr-fumarate, which has a face-centered cubic lattice (*fcc* topology) with three types of pore sizes of 0.48, 0.56 and 0.74 nm,[41] is isostructural with UiO-66(Zr).[5] A steep uptake between p/p_0 = 0.05–0.1 is observed, and a maximum capacity (up to 0.36 g g^{-1}) is reached at p/p_0 = 0.9.[5] MIP-200(Zr)[63] possesses 1D triangular (0.68 nm) and hexagonal (1.3 nm) channels and displays a type IV isotherm with a low inflection point at p/p_0 = 0.18, and minimal hysteresis is observed.[5] MOF-841(Zr)[37] has fluorite topology with a pore size of 1.33 nm and displays a type V isotherm with a low inflection point at p/p_0 = 0.22. A steep uptake (between p/p_0 = 0.20–0.30) and a maximum capacity (up to 0.51 g g^{-1}) are observed (Figure 5). The desorption hysteresis is absent.[5]

Co-CUK-1[64] has 1D infinite square-shaped channels with a pore size of 1.34 nm × 1.3 nm. Co-CUK-1 displays an S-shaped isotherm with a steep uptake at p/p_0 = 0.12. Minimal hysteresis is observed.[5] AlFFIVE-1-Ni (KAUST-8)[57] has 1D channels and displays a type I isotherm (Figure 5) which features a saturated uptake (up to 0.24 g g^{-1}) at a low relative pressure (p/p_0 = 0.05).[5] MWH-1(Zn)[56] has unique 2D narrow interlayer space and pore cavities (0.36 nm × 0.38 nm × 0.66 nm) sandwiched by the layers, which enable the full entrance of H_2O molecule.[65] MWH-1(Zn) displays a type I isotherm (Figure 5) which features a saturated uptake (up to 0.13 g g^{-1}) at a low relative pressure (p/p_0 = 0.03). Its structure remains stable when exposed to air for one year or immersed in hot water (393 K in a closed autoclave) for 7 days.[56]

4.1.2. Targeted MOF Synthesis Strategies

With the advanced development of material science, increasing synthetic and modification methods have been presented to create high-performance MOFs. To synthesize MOFs with potential for application in water-adsorption-based possess, the design schemes for synthesis variation of MOFs play an indispensable role. MOF synthesis strategies distinguished in this section are intended to produce on-purpose MOFs with optimal water-related properties.

Linker variation – Functionalised linkers. Modifying MOFs by functionalization of the linker with hydrophilic or hydrophobic groups can move the step to lower or higher relative pressures.[5,66] MIL-53(Al) shows a pronounced breathing effect triggered by water molecules, and the introduction of OH groups makes breathing possible at around p/p_0 = 0.75.[5] MIL-53(Al)-OH[67] features 1D channels with free dimensions varying between 1.7 nm × 1.2 nm and 1.9 nm × 0.8 nm, which attribute to the breathing behavior.[5]

The CAU-1(Al) family is constructed using functionalized terephthalic acid linkers.[68] Among them, CAU-1(Al)-OH[68] with OH functionalized linker has a body-centered cubic lattice (*bcu* topology) with two types of pore sizes of 0.62 and 0.86 nm. CAU-1(Al)-OH exhibits non-steep, S-shaped isotherms with an apparent hysteresis loop (Figure S1, Supporting Information). CAU-1(Al)-OH exhibits good recyclability over 500 water adsorption cycles.[68]

Zr-adip[69] is designed by incorporating hydrophilic nitrogen sites into MIP-200(Zr). Compared with MIP-200(Zr), the immobilized –NH– sites in Zr-adip improve the pore hydrophilicity and maintain its higher pore volume (0.47 cm^3 g^{-1} for Zr-adip and 0.40 cm^3 g^{-1} for MIP-200(Zr)).[69] The isotherm shape of Zr-adip (Figure S1, Supporting Information) is the same as that of MIP-200(Zr), but with significantly improved uptake capacity in the low relative pressure range (p/p_0 = 0.1–0.25). This MOF was stable for over 300 cycles.

Lu et al.[70] investigated the relationship between MOF structure and water sorption properties by altering pore size, surface area, and pore functionality in a family of isomorphic UiO-type MOFs. Thirteen isoreticular MOFs were synthesized, and it was found that the introduction of hydrophilic groups can improve water uptake and adsorption kinetics at low relative pressure,

while hydrophobic groups or pore size extension has negative effects. UiO-66(Zr)-N, functionalized with Lewis basic nitrogen sites, shows the highest water uptake and fastest adsorption rate at 298 K and $p/p_0 = 0.2$ among these MOFs, with a high coefficient of performance for cooling applications.

Zhu et al.[71] introduced a "pore-nanospace post-engineering" strategy to optimize the hydrophilicity, water-uptake capacity, and air-purifying ability of MOFs with long-term stability. By variant tuning of organic linkers carrying hydrophobic and hydrophilic groups in the pore-nanospaces of prototypical UiO-67(Zr), a moderately hydrophilic MOF (UiO-67-4Me-NH_2-38%) with high thermal, hydrolytic, and acid-base stability was screened out.

Through a deliberate adjustment of the linker in NU-1000(Zr) (using TBAPy-2 instead of TBAPy), ISO-NU-1000(Zr)[72] with blocked windows but large pores (1.3 and 3.2 nm) exhibits high water capacity (up to 1.1 g g^{-1}) and better cycle stability.

MIL-125(Ti)-NH_2[34] is deliberately prepared by decorating NH_2 groups on MIL-125(Ti)'s BDC linkers in order to get a more hydrophilic and robust framework.[5] MIL-125(Ti)-NH_2 has a 3D pore structure with two types of pore sizes of 0.6 and 1.2 nm, and displays an S-shaped isotherm with a steep uptake at $p/p_0 = 0.2$. Minimal hysteresis is observed.

Post-synthetic linker exchange. FDM-92(Al),[73] presented by replacing FDM-91(Al)'s weak $[Cu(HPyC)_2]^-$ moieties with BPDC linkers post-synthetically, possesses triangular 1D channels with an opening of 1.22 nm.[73] FDM-92(Al) shows non-steep, S-shaped isotherms with a small hysteresis loop (Figure S1, Supporting Information) and better cycling performance.

MOF-808(Zr)[37] exhibits good water capacity but quickly suffers a large capacity loss due to water-evacuation-induced pore collapse.[74] Halide-ion-loaded MOF-808(Zr)-Br[74] shows an improved performance in both water capacity (up to 0.70 g g^{-1}) and recyclability. MOF-808(Zr)$PDS_{1.7}$[75] and MOF-808(Zr)$NDS_{1.8}$[75] are presented by post-synthetic modification (PSM) of MOF-808(Zr). Their recyclability has been improved by di-sulfonic acid PSM, but the improvements in water capacities are limited (0.61 g g^{-1} for MOF-808(Zr)$PDS_{1.7}$ and 0.53 g g^{-1} for MOF-808(Zr)$NDS_{1.8}$).

Variation of the linker connectivity. Systematic linker variation is a synthesis approach, which ingeniously utilizes the diversity of reticular framework. Through the systematic synthesis and analysis of a series of MOFs, the best samples could be found. Gong et al.[76] utilized reticular chemistry to create a range of robust Zr-MOFs with a unique [2.2]*para*-cyclophane (PCP) scaffold. The PCP scaffold's functionalization ease enabled the synthesis of three carboxylate linkers, including one ditopic and two tetratopic, that assembled into a total of five Zr-MOFs. Finally, NU-913(Zr) stood out. Systematic variation provides a systematic approach to exploring new MOFs suitable for water-related applications.

Mixed linker synthesis – Multivariate MOFs. With the further study of water adsorption mechanism of MOFs, it has become a reality to modulate the binding strength of the first water molecules precisely and design the water uptake behavior deliberately by the multivariate MOF strategy.[4,77,78] The key to the multivariate MOF strategy is that the structures of the selected linkers should be similar, which enables crystallization of both linkers in the same crystal lattice, in order to avoid formation of a mixture of single-linker MOFs.[78] Hanikel et al.[4] prepared a series of multivariate MOFs by adjusting the ratio of $PZDC^{2-}$ to FDC^{2-} linker. With the increasing amounts of FDC^{2-}, the water isotherm step shifted continuously toward higher relative pressures and covered the entire range between the adsorption–desorption isotherms of MOF-303(Al) and MOF-333(Al).[4] (**Figure 6**(a))

Hanikel et al.[55] also proposed a linker extension strategy for generating MOFs with superior water-related properties. Compared with MOF-303(Al), MOF-LA2-1(Al) with the extended linker exhibits a ≈50% water capacity increase (Figure 5).[55]

Zheng et al.[78] highlighted the use of a multivariate strategy in making MOFs to control the hydrophilic nature of the pores, allowing for the tuning of regeneration temperature, enthalpy of adsorption, and water isotherm step. By introducing TDC^{2-} along with $PZDC^{2-}$ in the MOF backbone, nine multivariate PT-MOFs covering the entire linker mixing range were produced,[78] and demonstrated the ability to access a broad range of tunability between the adsorption–desorption isotherms of MOF-303(Al) and CAU-23(Al).

Polymorphism. Matemb Ma Netp et al.[11] described a new approach to adjust the hydrophilicity of MOFs by utilizing polymorphism in Al-MOFs. This involves creating MOFs using the *trans-* and/or *cis-* μ-OH-connectivity in chains of corner-sharing $AlO_4(OH)_2$ octahedra (Figure 6(b) and 6(c)). MIP-211(Al), made of *trans, trans*-muconate linkers and chains of *cis*-μ-OH-connected corner-sharing $AlO_4(OH)_2$ octahedra. In MIL-53(Al)-muc, the different chain structure of only *trans*-μ-OH-connected corner-sharing $AlO_4(OH)_2$ octahedra resulted in a shift of the step position of the water isotherm from $p/p_0 = \approx 0.3$ to ≈0.5. The authors used solid-state NMR and Grand Canonical Monte Carlo simulation to analyze the adsorption behavior of these two MOFs and found that adsorption occurs initially between two hydroxyl groups of the chains, favored by the *cis*-positioning in MIP-211(Al), resulting in a more hydrophilic behavior. The shift in the step position of the water isotherm from $p/p_{0=} \approx 0.5$ in MIL-53(Al)-muc to $p/p_0 = \approx 0.3$ in MIP-211(Al) (Figure 5) suggested that the polymorphism approach can effectively be used to tune the hydrophilicity of MOFs.

4.1.3. Other Strategies

Tan et al.[79] prepared ***mixed Al-based MOFs*** (CAU-10(Al)-H and Al-fumarate) by one-pot solvothermal method, which showed a controllable water uptake step tuned in the range of $p/p_{0=}$ 0.14–0.3. Different from the multivariate MOF strategy, the MOF synthesized by this method is a mixture of MOFs, but the effects of the two methods appear to be the same. Stassin et al. applied this mixed linker approach in flow synthesis of MIL-53 or MIL-68-type structure. By varying the linker ratio, the sorption properties could be adjusted, although the product structure was determined by the major linker fraction.[80]

By ***confining a hygroscopic salt*** in MIL-101(Cr) matrix, the composite sorbent LiCl@MIL-101(Cr),[81] shows a gradual water uptake with relative pressure up to 1.87 g g^{-1} at saturation (Figure S1, Supporting Information). The pores of the MIL-101(Cr) matrix can provide sufficient space for water storage, and LiCl, within the MIL-101(Cr)'s cages, perform chemical adsorption and desorption of water. Although the adsorption

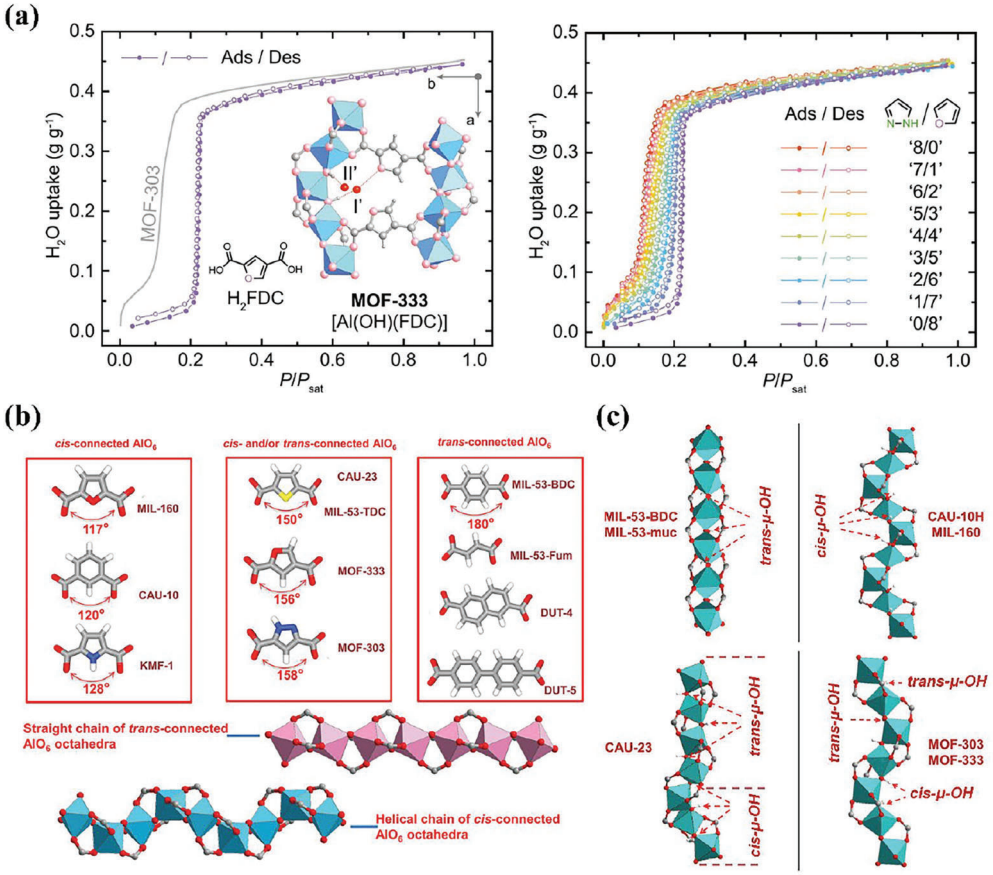

Figure 6. a) Water adsorption isotherms of MOF-333 and MOF-303 (grey) at 25 °C (left) and of their multivariate MOF series for different ratios of their linkers (right). The linker 2,4-furandicarboxylic acid (H_2FDC) and the pocket of MOF-333 with the first two adsorption sites (I′ and II′) are shown in the inset. Al, blue polyhedron; O in the framework structure, pink; O in H_2O, red; C and H, gray. Reproduced with permission.[4] Copyright 2021, American Association for the Advancement of Science (AAAS). b) Structures and opening angles of some dicarboxylate linkers that have been used to construct Al-MOFs made up of Al-O chains. Linkers that yield Al-MOFs made up of helical Al-O chains (left), linkers that yield Al-MOFs made up of mixed helical and/or straight Al-O chains (middle), and linkers that yield Al-MOFs made up of straight Al-O chains (right). Shared corners of AlO_6 octahedra are bridging μ-OH groups, which are trans-positioned or cis-positioned in straight or helical chains, respectively. Reproduced with permission.[11] Copyright 2023, Wiley-VCH. (c) Chains of corner-sharing AlO_6 octahedra in aluminum-based MOFs. The AlO_6 octahedra are (solely) trans-μ-OH-connected in MIL-53-BDC (top left), (solely) cis-μ-OH-connected in CAU-10H (top right), and mixed cis-μ-OH-/trans-μ-OH-connected in CAU-23 resulting in sections of straight and helical fragments (bottom left). The AlO_6 octahedra are alternatively trans-μ-OH- and cis-μ-OH- connected in MOF-303 resulting in a helical chain (bottom right). Reproduced with permission.[11] Copyright 2023, Wiley-VCH.

mechanism of LiCl@MIL-101(Cr) is not quite same as that of pure MIL-101(Cr), the combination of a hygroscopic salt and MOF is proven to be promising. This composite sorbent is stable for at least 20 adsorption cycles, indicating the LiCl has not leaked out from cages of MIL-101(Cr). Similarly, Yang et al.[82] used hollow spherical silica (HS) microcontainers to encapsulate different amounts of LiCl, named LiCl@HS-200, −500, and −700 resulting in similar capacities as with the MOF composite. In both cases, this encapsulation improves the effective surface area of the deliquescent fluid in the loaded sorbent, and hence the uptake release kinetics compared to a pure fluid, but a stepwise uptake is not present. Garzo-Tovar et al. synthesized composite salt in porous matrix by spray drying a mixture solution of $CaCl_2$ and reactants for UiO-66(Zr) called $CaCl_2$@UiO-66. The water isotherm showed a water uptake approximately proportional to the relative pressure up to ≈2.0 g g^{-1} (@90% RH), characteristic of a hygroscopic salt, but without a step. So the working capacity depends strongly on the operating conditions. Leaching was found negligible.[83]

The ***introduction of defects*** in UiO-66(Zr)[84] and CAU-10(Al)-H[85] significantly affect water adsorption properties that result in shifting steep water uptake and increasing water capacity. The defective Zr-Fum HT[86] (HT stands for hydrothermal synthesis using a water solvent) shows a steeper uptake and a larger capacity than solvothermal MOF-801(Zr).[86]

Based on the above overview, the water adsorption in the described MOFs is affected by their synthesis, structure, and functionalization. In this physical adsorption, water molecules nucleate on the hydrophilic sites in the pores of MOFs (a relatively low uptake at low pressure) followed by the formation of water clusters resulting in a steep uptake. This water sorption property is determined by the pore structure. The pore volume mainly determines the maximum working capacity as there is a linear relationship between pore volume V_p and water capacity q_{max}

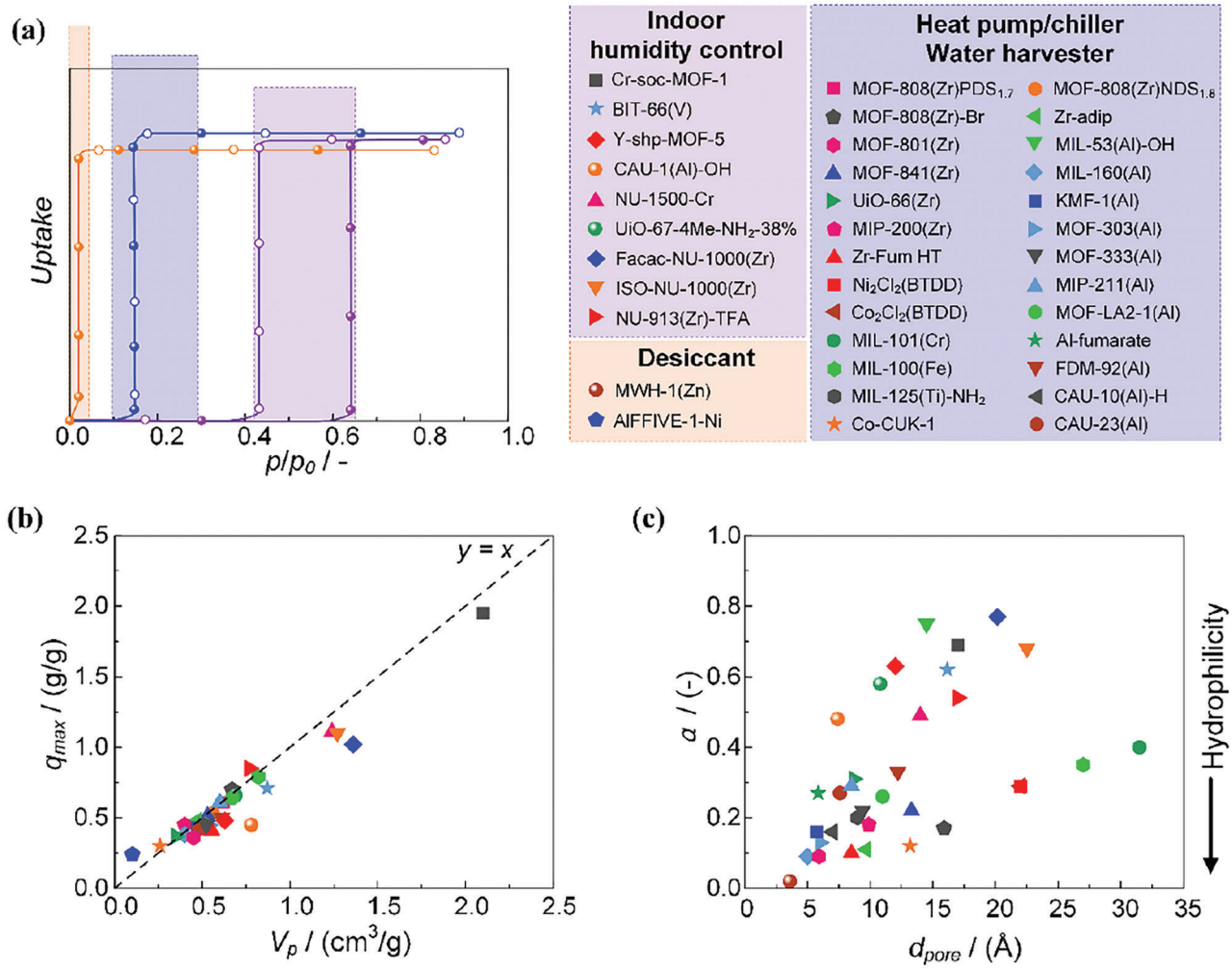

Figure 7. Properties of selected MOFs: a) Schematic diagram of water adsorption and desorption isotherms and indicated application ranges, b) relationship between pore volume and water capacity, and (c) collected data of inflection point at water adsorption step versus pore size.

(**Figure 7**(b)). The relationship between d_{pore} and α is less obvious (Figure 7(c)), but in general, smaller pore size and higher hydrophilicity are beneficial for a lower inflection point. 1D pores of ≈0.7 nm seem to be optimal for water cluster formation in the uptake step. Hydrophobic pores with larger sizes always need higher dispersive energy of water clusters to be sustained inside the pores.[90] Nevertheless, an excess of hydrophilic sites is not advantageous because then their contribution will start dominating the steep isotherms and require more energy for desorption. About pore shape, straight channels (see **Figure 8**) with negligible tortuosity are preferred to lower water diffusion resistance. Although MOFs with uniform 1D channels were intensively studied (27 out of 42 samples in Table 1), 2D and 3D ones are worth further exploration as their higher connectivity favors in principle the kinetics.

In addition to the extensive MOFs library, COFs that exhibit similar isotherm characteristics as MOFs may become alternatives without metals.[5,12,39,91–93] Among them, DHTA-Pa COF,[12] featuring a hydrophobic skeleton, suitable hydrophilic site density, and 1D channels, shows significantly high water diffusivity (**Figure 9**) and thermal conductivity (0.2620 W m^{-1} K^{-1} @298 K, compared with MOF-303: 0.1380 W m^{-1} K^{-1} @298 K, and MOF-801: 0.0953 W m^{-1} K^{-1} @298 K) which supports the material design strategy to achieve fast mass and heat transport kinetics. Furthermore, Sun et al. are the first to investigate the activation barriers for adsorption/desorption and intracrystalline diffusional transport.[12]

4.2. Scalable Synthesis of MOFs for Water Adsorption Applications

The synthetic scalability of MOFs with good water isotherm properties plays a crucial role in their wide practical applications. Developing facile, sustainable, and high-yield synthesis methods is the essential way for those MOFs to shift from laboratory scale to industrial scale. High-quality MOFs in terms of purity, crystallinity, porosity, and water-related performance should be ensured while synthesized at scale. The advantages and drawbacks of existing synthetic routes such as solvothermal, electrochemistry, microwave, ultrasonic radiation, green solvent reflux, room temperature stirring, steam-assisted transformation,

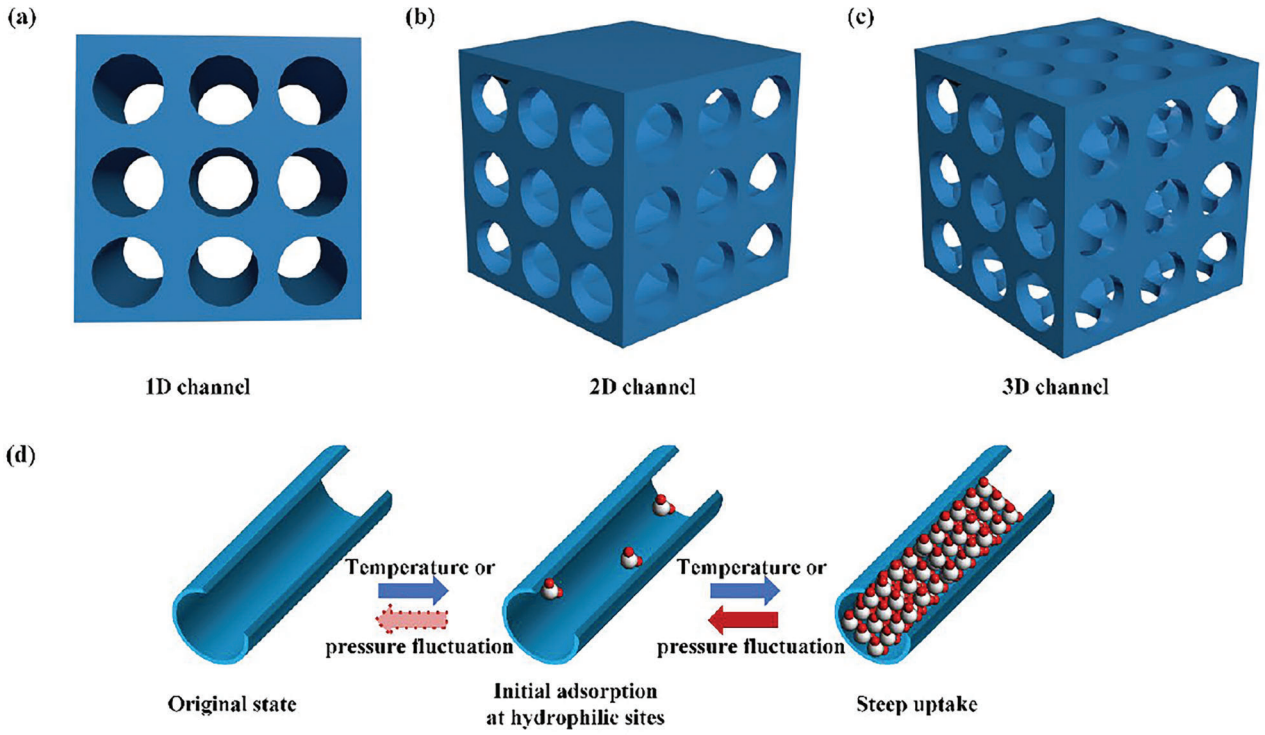

Figure 8. Schematic illustration of proposed ideal uniform pore structures in MOFs for water sorption: straight a) 1D channel, b) 2D channel, and c) 3D channel. d) Schematic diagram of the ideal water adsorption and desorption process with the regular ordering in a MOF channel.

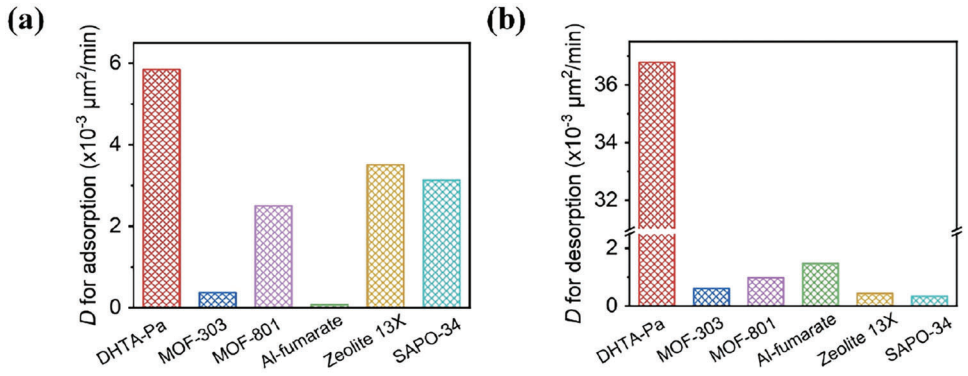

Figure 9. Calculated experimental diffusivities of DHTA-Pa COF, MOF-303(Al), MOF-801(Zr), Al-fumarate, Zeolite 13X and SAPO-34 under 30% RH. a) Water adsorption at 298 K and b) desorption at 333 K. Reproduced with permission.[12] Copyright 2023, Wiley-VCH.

mechanochemistry, flow chemistry, and spray-drying in terms of scale-up synthesis of MOFs have been well summarized in these reviews.[94–98] Most methods are still batchwise, but continuous synthesis is being developed. Several potential scalable synthesis methods of MOFs for water applications are summarized below.

4.2.1. Microwave Synthesis

Microwave synthesis has been proven to shorten the reaction time without compromising the yield and quality of lab-scale synthesis of MOFs, but the finite microwave penetration depth into the absorbing medium limits the reactor size and further the massive MOF synthesis.[94]

4.2.2. Ultrasonic-Assisted Synthesis

Ultrasonic-assisted synthesis can make the MOFs crystallize quickly, while the yield is not satisfactory.[94] Although the above methods have large limitations in the scale-up production of MOFs, using these methods as auxiliary means can also help to increase production (vide infra).

4.2.3. Green Solvent Reflux

Green solvent reflux, especially water refluxing, is a simple and green method suited for large-scale synthesis of MOF. Permyakova et al. synthesized MIL-160(Al) in a 2 L glass reactor

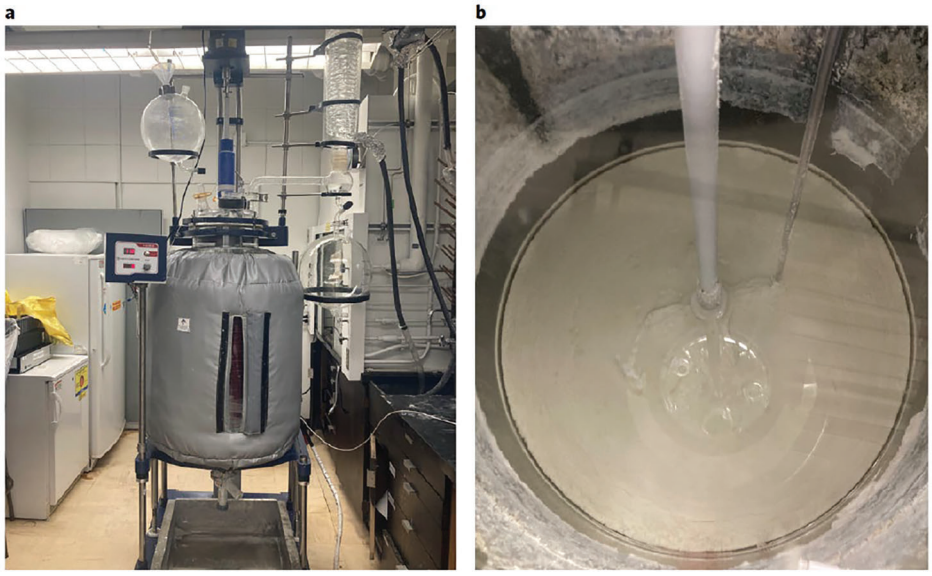

Figure 10. a) Photo of a kg-scale synthesis of MOF-303(Al) in a 200 L reaction vessel, and b) formation of slurry after refluxing for 6 h. Reproduced with permission.[88] Copyright 2022, Springer Nature.

by water refluxing as an illustration for large-scale syntheses.[99] Furthermore, Zheng et al. reported detailed green, water-based synthesis schemes for MOF-303(Al) at the gram and kilogram scales.[88] Compared with solvothermal, flask-scale reflux, and microwave methods, vessel-scale reflux method showed a MOF-303(Al) productivity of 3.5 kg per batch with 91% yield, with a performance equivalent to that produced at a small-scale (**Figure 10**). Vessel-scale reflux has also been further successfully applied for green synthesis and scale-up of CAU-23(Al), MIL-160(Al), MOF-313(Al), CAU-10(Al) and Al-fumarate by the same team.[100] In addition, using water and alcohol mixtures in a certain proportion gives MOFs with high yields and space-time-yields.[94] Lenzen et al.[101] realized a high 95% yield at 0.5 kg-scale of CAU-10(Al)-H by employing 5 vol% ethanol aqueous solution reflux. Green solvent reflux method gives remarkable yields and space-time-yields in the scale-up production of Al-based MOFs (**Table 2**).

4.2.4. Room Temperature Synthesis

Room temperature synthesis is an innovative, simple, efficient, cheap, and environmentally friendly method to produce MOFs.[94] Dai et al.[102] presented a one-step synthesis method of MOF-801(Zr) in a 5 L stirred pilot scale system at room temperature which showed a space-time-yield of 168 kg day^{-1} m^{-3}. Dai et al.[103] also presented the scalable room temperature synthesis method of MOF-808(Zr) nanocrystals with a tuning size from 35–850 nm.

4.2.5. Mechanochemical Synthesis

Mechanochemical synthesis is the process of grinding solids to facilitate quantitative chemical reactions which can synthesize MOFs efficiently.[94] Karadeniz et al.[104] proposed a scalable and continuous mechanochemical method to produce UiO-66(Zr) and MOF-801(Zr) using a twin screw extruder with a small amount of water added during the grinding process. Crawford et al.[105] realized the production of Al-fumarate by using a twin screw extruder and exhibited an outstanding space-time-yield of 27 000 kg day^{-1} m^{-3} which is higher than BASF's hydrothermal method.[106]

4.2.6. Continuous Flow Chemistry Synthesis

Continuous flow chemistry synthesis enables chemical reactions to occur in continuous flow rather than batchwise and has already been applied for scalable synthesis of MOFs.[80,94,95,107] Generally, flows of linker and inorganic precursor solutions are mixed in a small tube of sufficient length operating at the required temperature and residence time to allow for the MOF synthesis. The classical lengthy multi-day synthesis and high production costs have prevented widespread implementation of Ni_2Cl_2(BTDD) in spite of its good water-related performance.[42] Bagi et al.[48] reported a continuous synthesis process for Ni_2Cl_2(BTDD) in a flow reactor operated in so-called Taylor flow (**Figure 11**). Droplets of the synthesis mixture are injected in a continuous flow of a heated oil but do not mix and move forward in the small tube. Due to wall friction, the droplets are internally well mixed and in this slug flow mode, they all have the same residence time for synthesis. In this way, the residence time distribution as normal for laminar flow is avoided.[108] Compared with the batch process (shown in Table 2), a continuous process can achieve higher yields and shorter crystallization times. Flow reactor has high efficiency and rapid heat and mass transfer, which provides an opportunity for rapid and large-scale synthesis of MOF. Continuous flow synthesis can be assisted by microwave heating and ultrasonic amplification.[94] Taddei et al.[109] proposed a combination of microwave heating and continuous flow technology and realized the synthesis of UiO-66(Zr) and MIL-53(Al) with

Table 2. The information for scalable synthesis of selected MOFs.

MOF	Solvent and volume	Conditions	Dry MOF obtained per batch [g]	Yield [%]	Space-time-yield [kg day^{-1} m^{-3}]	Reference
Al-fumarate	No solvent	Mechanochemical synthesis	–	–	27 000[a)]	[105]
Al-fumarate (Basolite A520)	H_2O (N.A.)	–	–	98	> 3600	[106]
Al-fumarate	H_2O (50 L)	Reflux, 6 h	2970	94	238	[100]
CAU-10(Al)	H_2O (50 L)	Reflux, 6 h	3810	92	305	[100]
CAU-10(Al)-H	C_2H_5OH aqueous (5 vol%, 8.4 L)	Reflux, 10 h	500	95	–	[101]
CAU-23(Al)	H_2O (50 L)	Reflux, 6 h	3610	84	289	[100]
MIL-53(Al)	H_2O (91 mL), DMF (391 mL)	Continuous flow & microwave heating	4.0	65	3437	[109]
MIL-160(Al)	H_2O (50 L)	Reflux, 6 h	3640	92	291	[100]
MIL-160(Al)	H_2O (75 mL)	Reflux, 24h	14[b)]	93	185	[99]
MOF-303(Al)	H_2O (50 L)	Reflux, 6 h	3590	91	287	[88,100]
MOF-313(Al)	H_2O (0.5 L)	Reflux, 6 h	38	96	304	[100]
MOF-801(Zr)	H_2O (4 L)	Room temperature stirring, 5.5 h	234	88	168	[102]
MOF-808(Zr)	H_2O (1.67 mL)	Room temperature stirring, 5 h	10	98	2516	[103]
UiO-66(Zr)	CH_3COOH (103 mL), H_2O (26 mL), DMF (471 mL)	Continuous flow & microwave heating	17.5	94	4899	[109]
UiO-66(Zr)	BDC:H_2O:DMF = 1:40:135	Spray-drying & continuous flow-assisted	–	70	19.6	[110]
Ni_2Cl_2(BTDD)	DMF:CH_3OH:HCl = 1:0.5:0.38	Continuous flow 140 °C, 1 h	–	≈80	12.24	[48]
Ni_2Cl_2(BTDD)	DMF (0.2 L), C_2H_5OH (0.2 L)	Solvothermal 65 °C, 10 days	0.3	87	0.1	[42,100]

[a)] This value did not include washing and drying steps, only reaction time was considered. The other space-time-yield values listed in the table have taken the product purification process into account; [b)] This synthesis method was scaled-up to 400 g MOF powder per batch while yield and space-time yield were unknown.

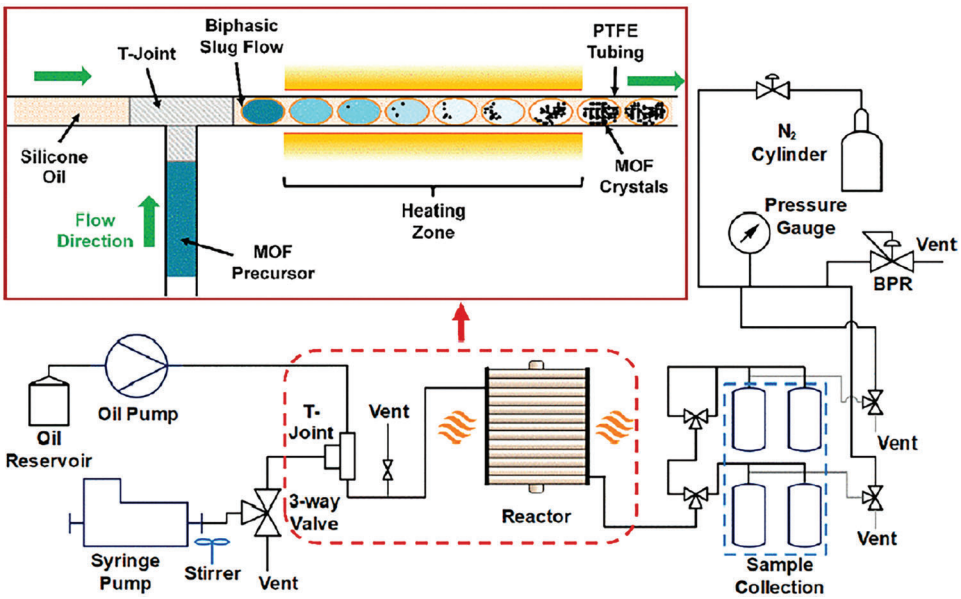

Figure 11. Continuous synthesis of Ni_2Cl_2(BTDD) in Taylor flow (or slug flow) mode suitable for scale-up synthesis. Reproduced with permission.[48] Copyright 2021, American Chemical Society.

high quality and yields. Also, spray-drying provides a solution for the synthesis of MOFs, COFs, and related composites.[17] By combining spray-drying and continuous flow-assisted synthesis, Garzón-Tovar et al. achieved the continuous production of UiO-66(Zr).[110]

As shown in Table 2, the successful scale-up of these MOFs demonstrates the feasibility of commercializing MOFs as water sorbents and contributes to a wide range of applications. Clearly, besides the yield or space-time-yield, availability, cost, toxicity, safety and environmental impact of synthesis methods should be taken into account.[97] Synthesis methods such as green solvent reflux of Al-based MOFs and continuous flow synthesis of various MOFs show remarkable potential for scale-up production and market availability. Both are promising and worthy of further exploration.

5. Applications

Reallocation of heat and cold through water ad- and desorption is deemed a green process with lower operating costs compared to conventional techniques (e.g., vapor compression cycles for cooling), although investment is still higher.[111–114] The thermodynamics and working principle of heat pump/chiller has been well summarized in our earlier reviews.[5,6] Following this line, only updated literature is included here. Besides the thermodynamics, the kinetics of adsorption–desorption is another critical parameter for practical application of this cyclic operation, determining the cycle times. The adsorption kinetics can be improved by modulating the pore structure and surface hydrophilicity.[115,116] Generally the water uptake by the MOF powder is fast, and convective or diffusive supply of water vapor is limiting, resulting in the development of concentration gradients on the MOF crystal, composite particle, and device level during operation.[5,19] Furthermore, this interferes with the associated thermal effects in combination with the poor thermal conductivity of MOFs. At higher water concentrations heat transport becomes the controlling step for adsorption-desorption cycles. However, in AWH, due to the low concentration of water, adsorption heat is easily dissipated in the large air excess, and this does not dominate the rate during adsorption. Here, the recent improvement in desorption kinetics by localized eddy current heating (LECH) is described. Emerging applications in air conditioning (humidity and temperature control), desiccation, and water harvesting are summarized as well. Potential other applications are suggested in each section. It is emphasized that although in all applications moisture handling is the same primary activity, the targets are different (e.g., freshwater production versus comfortable air), and the system or device design cannot be blindly copied from one to another application, whereas the ideal sorbent development follows nevertheless the same principle targeting steep uptake, high working capacity, fast kinetics, easy regeneration, and stability.

5.1. Kinetics Aspects

5.1.1. Stimulated Desorption

The rate of adsorption and desorption (kinetics) is crucial to determine the time required for completion of the adsorption-desorption cycle, which is depending on the interaction between the adsorbent and the adsorbate. The Linear Driving Force model has been widely used to describe the kinetics of an adsorption process because it is attractively simple and applicable to a wide range of adsorbents.[117,118] According to this approximate model, the adsorption rate is proportional to the driving force (local difference between equilibrium loading and averaged instantaneous particle loading) and an apparent diffusivity and is inversely related to the particle size or thickness of MOF coating. The same holds for desorption. Although effective, local particle and column concentrations are averaged in the model and detailed characteristics like adsorption heterogeneity, intraparticle concentration profiles, and kinetics are thereby lost.[119] So, the incorporation of hydrophilic species (Li-ions) to improve adsorption kinetics of MOFs will not be directly evident from the model formulation, although it is effective for Al-fumarate and MIL-101.[120,121] The incorporation of hydrophilic CHA zeolite also increased the water uptake speed of Al-fumarate-CHA by 1.7 times at 60°C and 5 kPa.[120] However, the regeneration of such composites required higher temperatures, increasing energy consumption. Sun et al. are the first to study the intrinsic energy barriers involved in water ad- and desorption and diffusion, by comparing COF, MOFs, and zeolites, showing the advantages of MOFs and especially COF.[12]

The rather low thermal conductivity of MOFs is the critical parameter limiting the desorption kinetics.[12,122–124] For instance, the thermal conductivity of single crystal MOF-5, ZIF-8, and UiO-66 powder is low, 0.32, 0.33, and 0.11 W m^{-1} K^{-1}, respectively.[125–127] This is in the same order of magnitude as the intrinsically poor thermal conductivity of a packed bed.[14,128] For MIL-101 and Al-fum beds this varies in the range 0.056-0.12 W m^{-1} K^{-1}.[89,129,130] Hot surface-heating with electrical heating stripes represents the most common heating manner to drive water release from MOFs sorbents. However, given the intrinsic thermal insulating nature of porous MOF sorbents, such traditional hot-surface heating would inevitably result in uneven and inefficient heating of sorbents, causing slow water release and high energy consumption. Kim et al.[131] reported the thermal efficiency of MOF-801 (*i.e.*, the product of latent heat of water and mass of harvested water per unit input solar energy) was 14% for atmospheric water generator, which can produce 0.25 L_{H2O} $kg^{-1}{}_{MOF}$ day^{-1} at a relative humidity of 10–40%. An alternative is preheating the (much smaller amount of) air used in the desorption stage.[132]

To overcome these issues and realize fast water release and high energy-efficiency, the stimuli-responsive MOF composites by embedding versatile functional components (metal/ carbon foams, magnetic nanoparticles, carbon paper/fibers, and MXene nanosheets) would be a better alternative.[24–29] Upon exposure to external stimuli such as magnetic field, electric current, light, and combinations thereof, such embedded functional components help generate a rapid and localized uniform heating within MOF particles. Tao et al.[25] adopted localized eddy current heating (LECH) to overcome the intrinsic thermal insulation nature of the porous metal–organic framework (**Figure 12**). In particular, since such localized heating takes place within the MOF matrix, the system heat loss can be effectively mitigated, making the localized heating-driven MOFs regeneration more energy efficient.

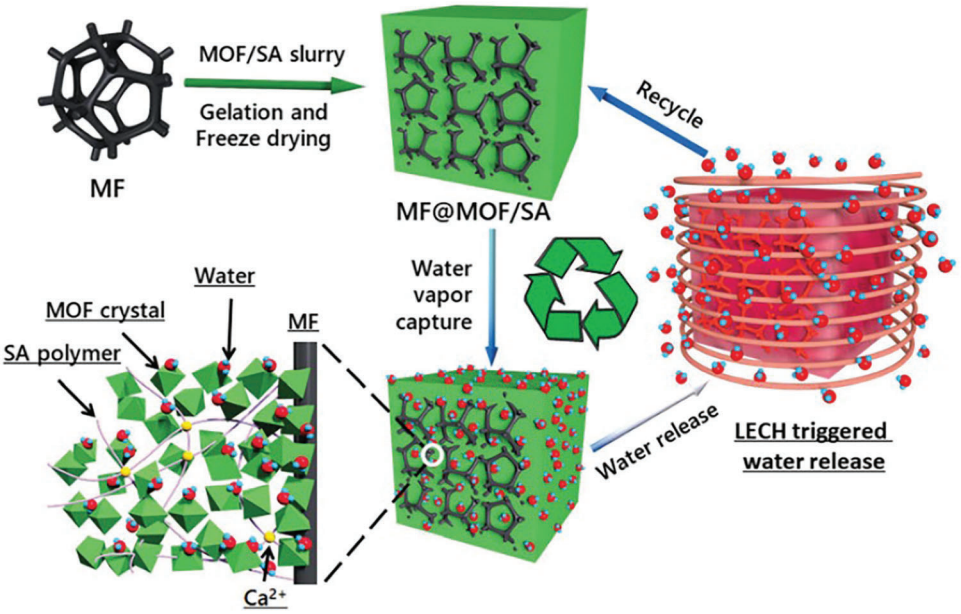

Figure 12. Schematic illustration of the preparation of MF@MOFs, water vapor capture, and LECH-triggered water release from MF@MOFs. (LECH, localized eddy current heating; SA, sodium alginate; MF, metal foam). Reproduced with permission.[25] Copyright 2021, Royal Society of Chemistry.

Table 3. Different water release methods for adsorption water harvesting (AWH).

Material	Heating method	Water productivity [L_{H2O} kg_{MOF}^{-1} day^{-1}]	Energy consumption [kWh L_{H2O}^{-1}]	Working condition	Reference
Localized heating					
Carbon fiber/Al-fumarate/SA (sodium alginate) monolith	Localized electrical heating	1.7	4.4	Indoor	[135]
Carbon fiber/Al-fumarate/SA monolith	Localized electrical heating	1.2	6.2	Outdoor (1.3–13.9 °C, 30–75% RH)	[135]
MOF monolith (Al-fumarate embedded in a carbon scaffold)	Localized electrical heating	1.95	1.57	23–26 °C, 28–38% RH	[24]
MOF monolith (Al-fumarate, multiwalled carbon nanotubes, cross-linked SA)	Localized solar heating and electrical heating	1.4	2.3	Indoor	[28]
MOF@MF monolith (MIL-101(Cr), SA)	Localized eddy current heating	2.2	–	60% RH	[25]
Traditional heating					
MOF-801	Electric heater (desorption air)	1.8	5.3	10–30% RH	[132]
LiCl-Carbon fiber felt composite	Electric heater (sample bed)	0.32	2.3	One-layer one-hour case	[136]
Structured activated carbon fiber-LiCl composite	Electric heater (desorption air)	0.55	2	Large fluctuations in humidity	[137]

Driven by such localized heating, rapid water release from MOFs (*e.g.*, MIL-101(Cr)) can be easily achieved and reach a water productivity of 2.2 L_{H2O} $kg^{-1}{}_{MOF}$ day^{-1} (60% RH).[25] (**Table 3**) This approach synergistically enables fast-cycling of water adsorption and desorption on MOFs, improving remarkably the heating or cooling power of heat pump/chiller.[133,134]

5.1.2. Application Formulation

Shaping the MOF powder is essential to demonstrate a scaled-up application in the form of a packed bed, rotary wheel, and desiccant-coated heat exchanger (DCHE).[138,139] In the first two water removal is targeted but faces the adverse effect of

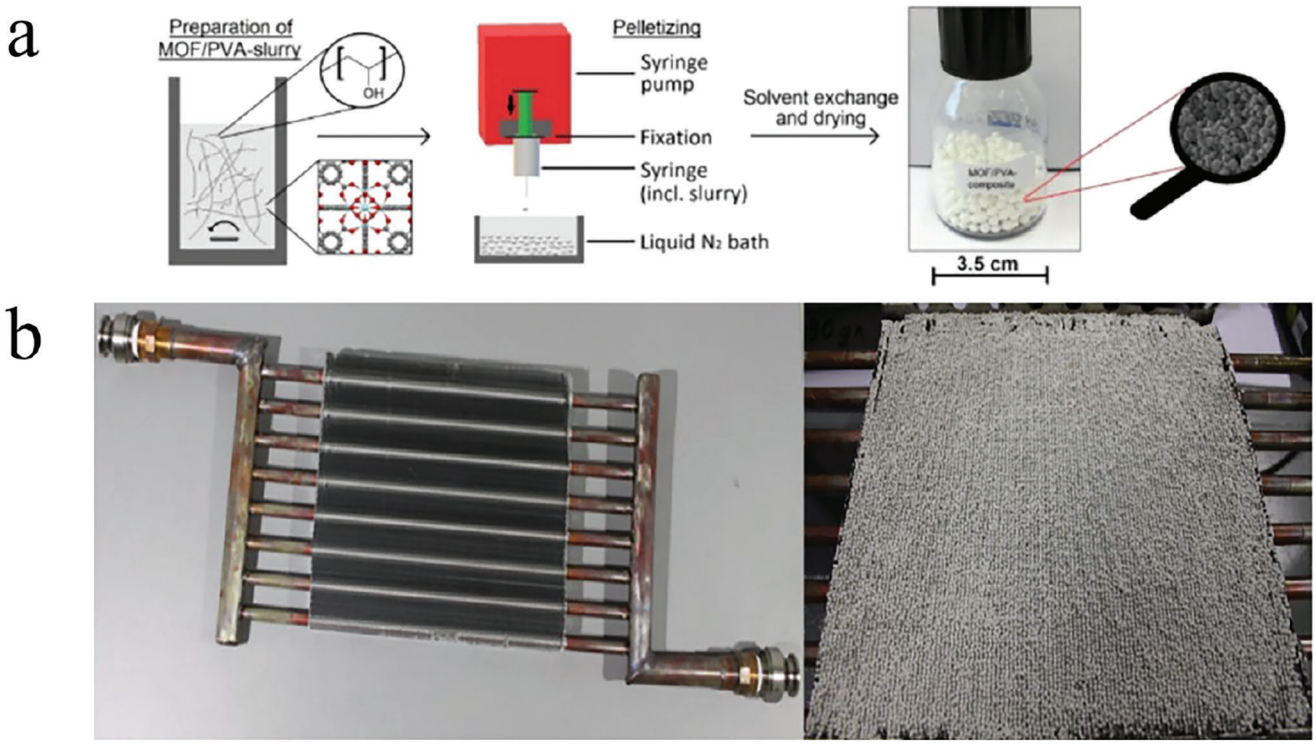

Figure 13. a) Example of fabrication process of pellets including the preparation of PVA/MOF-slurry. b) Pipe-lamella heat exchanger unfilled (left) and filled (right) with pellets. Reproduced with permission.[141] Copyright 2019, American Chemical Society.

adsorption heat on the adsorbent loading,[140] while with DCHEs energy-efficiency is targeted. Gökpinar et al.[141] used poly(vinyl alcohol) (PVA) as binder for Al-fumarate (Basolite A520), Zr-fumarate (MOF-801), MIL-160(Al), and UiO-66(Zr) to manufacture millimeter-sized pellets of for PVA/MOF (20/80 wt.%) through freeze granulation, to be packed between the pipe-lamella of a heat exchanger (**Figure 13**). The specific cooling power (SCP) ranging from 349 up to 431 W kg^{-1} is superior compared to the currently commercially used silica gel grains (50–230 W kg^{-1}) in adsorption heat pumps (**Table 4**). Farrusseng et al. produced Al-fumarate beads using alginate as binder and also for packing a heat exchanger, studying the mass and heat transport.[18] Bezrukov et al. manufactured AWH paper from a MOF powder-cellulose fiber slurry, preserving the excellent mass transport properties of the MOF powder due to the macropores of the composite.[19]

Other effective methods such as slurry dip coating, spray coating, and direct synthesis on a surface also have been used to coat MOFs on heat exchangers.[142] Lee et al. used dip coating with an epoxy binder to coat a finned tube heat exchanger with aluminum fumarate. They found that increasing the coating thickness from 0.05 to 0.2 mm and the cycle time from 150 to 300 s improved the dehumidification performance by 113% and 131%, respectively. Ge et al.[143] used spray coating (binder-free) to load Al-based MOFs (MIL-96 and MIL-100) onto a microchannel heat exchanger. Betke et al.[144] even synthesized CAU-10 directly onto open-cellular alumina foams under continuous rotation of the reaction vessel leading to 190–325 µm coating layers. The foam composite improved the thermal conductivity to 0.90–1.78 W m^{-1} K^{-1}.

The development of material shaping technology of MOFs has promoted their application in humidity and temperature control. The emergence of the binder-free method that enables high-performance MOF coating,[13,145] opening large-scale applications of MOFs. However, the widespread use of MOFs in devices is still impeded by relatively high costs and limited availability on a large scale.[7]

An underexposed aspect is the potential performance degradation of the MOF after the shaping process, depending on the technique used. Chen et al., using powder compression, observed a 50% loss of working capacity, and 10–20 times longer cycle times.[146] This aspect must be given standard attention in development studies.

5.2. Air Conditioning

5.2.1. Humidity Control

Indoor relative humidity (RH) is of great importance in human daily life. The proper habitable indoor RH recommended by the American Society of Heating, Refrigerating, and Air-Conditioning Engineers (ASHRAE) falls in the range of 45% to 65% RH.[58] The MOFs, such as Y-shp-MOF-5,[58] Cr-soc-MOF-1,[35] BIT-66(V),[10] CAU-1(Al)-OH,[68] CAU-1(Al)-CH_3,[68] NU-1500-Cr,[59] UiO-67-4Me-NH_2-38%,[71] Facac-NU-1000(Zr),[87] ISO-NU-1000(Zr)[72] and NU-913(Zr)-TFA,[76] possess typically S-shaped water vapor isotherms with the adsorption and desorption branches featuring a pronounced hysteresis and located in the middle of the ASHRAE recommended range

Table 4. Examples of devices based on water adsorption in MOFs.

Material	Device type	Binder	Coating method	Adsorption capacity [g g^{-1}]	Working conditions	Reference
Desiccant-coated heat exchanger (DECH) and Adsorption water harvesting (AWH)						
CAU-10(Al)-Hm	Reticulated open-cellular alumina foams	Binder-free	Direct synthesis	0.14	–	[144]
Al-based MOFs (MIL-96 and MIL-100)	Microchannel heat exchanger	Binder-free	Spraying coating	0.35	20 °C and 70% RH	[143]
Al-fumarate	Fin-tube heat exchanger	Mixture of epoxy with water and ethyl alcohol	Dip coating	0.40	27 °C and 49% RH	[147]
MIL-101/CFP-70	Desiccant wheel	Binder-free	Brush coating	0.25	20 °C and 70% RH @v_{air} = 0.1 m s^{-1}	[148]
Cu-BTC @ (HKUST-1)	Fin-tube heat exchanger	–	–	0.42	25 °C	[149]
Al-fumarate	Desiccant wheel	Epoxy	Dip coating	0.4	19–35 °C and 49% RH	[150]

Material	Device type	Binder	Coating method	Coefficient of Performance	Specific cooling power [kW kg^{-1}]	Working conditions	Ref.
Adsorption heat pump (AHT)							
MOF-801	Metal support that imitates a heat-exchanger fin	Binder-free	Shaped as pellets	0.67	1-2	T_{ads} = 30 °C @ T_{eva} = 5 °C	[151]
NH_2-MIL-125	Adsorbent bed (metal plate)	Binder-free	Shaped as pellets	–	0.4–2.8	P = 2.36 kPa, T_{ads} = 40 °C, T_{des} = 110 °C	[152, 153]
Al-fumarate	Wire fin heat exchanger	Hydroxyethyl Cellulose	Dip coating	0.32	0.68	10 wt% binder @25 °C	[154]
Al-fumarate (MOF-A520)	Fin-tube heat exchanger	A mixture of vinyl acetate and distilled water in an equal weight ratio	Spraying @coating	0.44	–	30 °C and 80% RH	[155]
Al-fumarate (Basolite A520)	Finned heat exchanger with aluminum fins pressed onto copper tubes	Polysiloxane	Dip coating	0.61	1.39	p/p_0 = 0.48 @25 °C	[156]
Al-fumarate	Fin-tube heat exchanger	Organic silicone	Dip coating	0.6	1	p/p_0 = 0.4	[157]
TiAPSO SCT-323	Aluminum plate with self-adhesive stencils	Wacker SilRes MP50E	Brush coating	–	–	δ = 470 µm	[158]

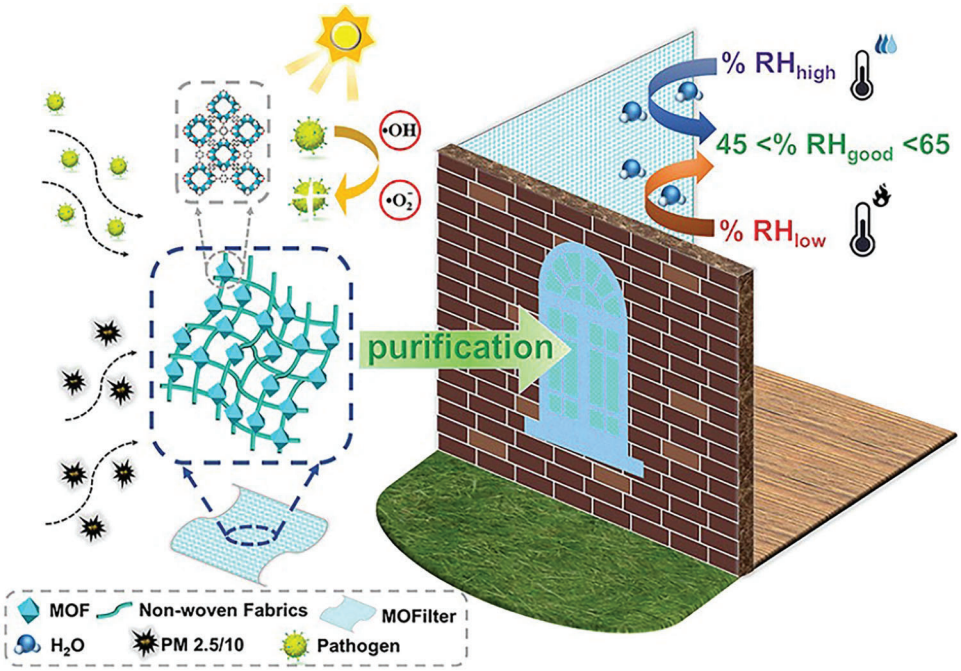

Figure 14. Suggested combined control of indoor humidity and air purification using MOFs. Reproduced with permission.[68] Copyright 2020, American Chemical Society.

at room temperature. These properties enable MOF to rapidly adsorb water vapor at high RH levels (>65%) or release water vapor quickly at low RH levels (<45%), thus realizing the function of autonomous indoor humidity control.

Interestingly, UiO-67-4Me-NH_2-38% shows also a good performance to preferentially capture hazardous gases, such as formaldehyde, benzene, toluene, normal-hexane, and ammonia, under high RH conditions, and can be easily regenerated by nitrogen purging at 100 °C for 2 h for reuse.[71] BIT-66(V) demonstrates a unique photocatalytic bacteriostatic performance under visible light,[10] which is conducive to the application of MOFs as humidity control adsorbents especially in confined spaces. Besides, CAU-1(Al)-OH presents an excellent photocatalytic killing efficiency against *E. coli*, and the air filter coated with CAU-1(Al)-OH can buffer the sudden humidity changes caused by outside air infiltration and effectively reduce the pollution of bioaerosol or particulate matter (**Figure 14**).[68] So, these MOFs possess an indoor air purification function which makes them superior in humidity control.

In addition to home indoor humidity control, MOFs could be well applied at other RH working ranges. For example, the RH range of microelectronics industry is 10–30%, and the RH range of artworks storage in musea is 20–30%.[159]

Other MOFs, such as Al-fumarate, MIL-100(Fe), and MIL-101(Cr), with lower inflection points and minimal hysteresis also have broad prospects in applications in industrial and commercial dehumidification systems in order to improve energy utilization efficiency of the evaporative cooler.[160] By arranging several desiccant wheels loaded with different MOFs according to the steep adsorption trigger point from high to low, the performance of the dehumidification system can theoretically be improved.[161]

5.2.2. Temperature Control

The current refrigerator cooling systems based on vapor compression cycles consume primary energy and contribute to global warming. Nowadays water-evaporative cooling by adsorption heat transformation (AHT) is deemed a green and low-cost technology, energy-saving, and environmentally friendly.[141] A prime example is the application of an adsorption chiller for the high-performance computer CooLMUC-2 at the Leibniz Supercomputer Centre (LRZ).[162] A compact ten-fold smaller and silent cooling system without moving parts was obtained consuming 40% less energy. Silica gel was used as sorbent. A techno-economic analysis indicated that a pay-back time of 6 years would be possible (using an electricity price in 2016 of 0.16 € kWh^{-1}).[114] Optimizing the adsorption chillers for data centers, i.e., lower regeneration temperatures, would improve the performance further. MOFs would be excellent candidates to replace silica.

For closed systems various MOFs have been extensively assessed for adsorption-based heat pump applications in our recent reviews based on their key performance indicators of thermal efficiency, COP_C (coefficient of cooling performance), and specific cooling power (SCP).[5,6]

Recent work of Gkaniatsou et al.[157] a full-scale adsorption chiller with different Al-MOFs (*i.e.*, MIL-160, CAU-10, and Al-Fum), and regeneration by solar heating was tested. All MOFs showed a thermal efficiency of 0.6–0.65 and high specific cooling power (SCP) of 1–2 kW kg^{-1}. A wire-finned heat exchanger loaded with aluminum fumarate exhibited a SCP up to 0.69 kW kg^{-1}. Compared with the packed heat exchanger, these parameters were increased by 53%.[154] A composite $CaCl_2$@UiO-66(Zr) synthesized by Garzon-Tovar et al.[83] showed an SCP of 0.63 kW kg^{-1}($CaCl_2$, 53% w/w) and excellent performance with

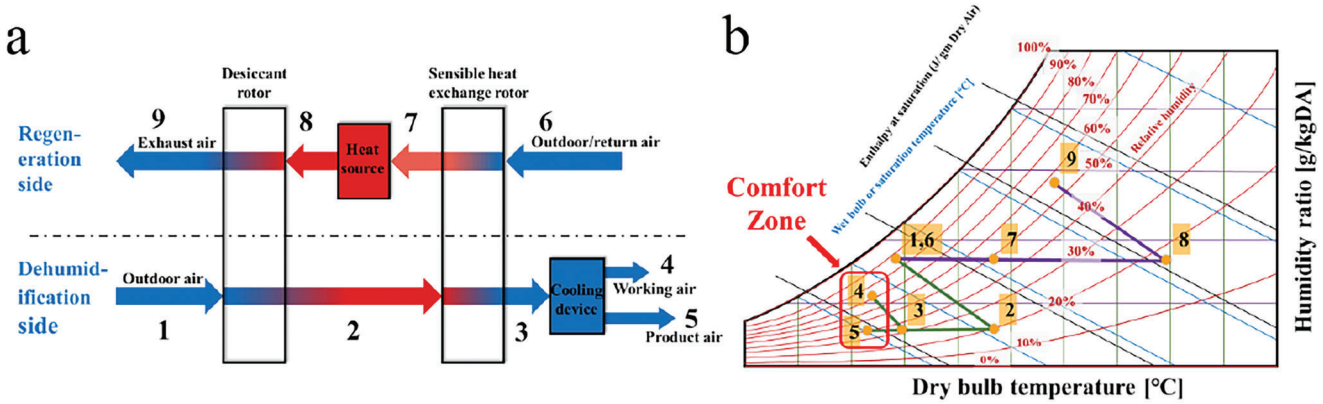

Figure 15. a) Schematic diagram of a rotary DAC system and the two followed pathways (1→4,5 green and 6→9 purple) of the air treatment in the psychrometric chart. Reproduced with permission.[165] Copyright 2015, Elsevier.

a COP_C of 0.83.[83] However, due to the isotherm shape, this composite material requires higher regeneration temperatures (≈110 °C).

In air conditioning, an open system, both humidity and temperature are controlled. Air conditioning accounts for 15% of global energy consumption.[163] The latent heat load of moisture in the air accounts for 40% of the total load of the air conditioner, depending on the geographic location.[164] Here, we focus on desiccant air-conditioning (DAC),[165–170] where MOFs could be applied. This usually consists of a desiccant unit (wheel/rotor or block type), a heat exchanger, a heating source, a low-cost cooling source, and some associated accessories. This is depicted for a rotary DAC in **Figure 15**(a).[165] Outdoor air becomes hot dry air through desiccation stage 1–2, and the heat is recovered during 2–3 and used for pre-heating return air in stage 6–7. This increases the coefficient of performance (COP) of the system. After further heating, this air regeneration occurs in stages 8–9. As desiccant MOFs could play an excellent role as they can be regenerated at low temperatures, e.g. by solar heat.[166,170] The dried air can be further cooled by evaporative cooling, including the efficient M-cycle.[165,171,172] The pathway of the air–water vapor stages in the psychrometric chart is outlined in Figure 15(b). Habib et al.[172] simulated the stand-alone DAC system and obtained a COP of 0.55. The combination of DAC with M-cycle further improved the performance of cooling. Pandey et al.[173] proposed a novel desiccant air conditioning/dry desalination system with a COP of 0.85–0.92, nearly twice the COP of the stand-alone DAC system.[166,167] The dehumidification also improves the efficiency of M-cycle cooling system in regions with high humidity.[174] Shahavi et al. compared by modeling the performance of a system of a desiccant wheel combined with indirect evaporative cooling (IEC) for three MOFs (CAU-10, CAU-23, Co_2Cl_2(BTDD)) and silica gel, based on their experimental adsorption isotherm data.[175] For all explored conditions the MOF coatings outperformed silica gel because of their lower regeneration temperature and larger humidity driving force for desorption during regeneration, resulting in shorter regeneration time. The optimal regeneration temperature range for the MOFs (45–75 °C) allows the use of solar or waste heat.[175] In a multi-stage wheel arrangement, the authors show a further regeneration and dehumidification efficiency improvement with up to 20 and 40%, approaching the theoretical maximum energy performance for desiccant dehumidification.[161]

Further applications of MOF-based DACs are envisioned by retrofitting existing devices in vegetable storage, greenhouse air-conditioning, industrial air-conditioning, livestock air-conditioning, agricultural product drying, etc.[176]

5.3. Water Production

5.3.1. Water Harvesting

Harvesting clean water from the atmosphere[177] provides a potentially sustainable solution to alleviate the shortage of water resources in arid regions ("water out of thin air"). Adsorption-based atmospheric water harvesting (AAWH) technology is currently known to be suitable for desert and arid regions.[178] The working principle of AAWH can be simply decomposed into three steps: the water vapor from an arid atmosphere is first enriched in the adsorbent, then desorbed initiated by either a temperature or a pressure swing, and finally collected by condensation. Efficient water harvesting requires that adsorbents can adsorb and release sufficient water easily and quickly. Hygroscopic salts (LiCl, $CaCl_2$, etc.) have the advantage of low cost, affinity for water at low relative humidity and high capacity, but would deliquesce easily,[179] resulting in slow kinetics and loss of a steep uptake.[81,82,180] Hydrogels have high water capacity and low regenerative energy, but stability still needs to be improved.[179] MOFs with excellent water adsorption/desorption properties, high water capacities, and good stability are candidates for AAWH and have been successfully employed as adsorbents to harvest water from arid air.[181,182] According to the daily working frequency of adsorbent (MOF) and the way of water desorption and condensation, the AAWH devices (**Table 5**) can be divided into passive monocyclic and active multicyclic.[181]

The "passive" monocyclic AAWH device operates through a cyclic process that takes advantage of the changes in relative humidity (RH) caused by the daily change in temperature. During the night, when the temperature drops and the RH is relatively high, the device adsorbs water vapor. The adsorbed water is then released during the day, as the adsorbent is exposed to direct

Table 5. MOF-based adsorption-based atmospheric water harvesting (AAWH) devices.

Material	Adsorbent shape	Operational stability	Assistant	Daily water productivity	Reference
Passive monocyclic AAWH device					
MOF-801(Zr)	Powder bed	Stable operation for a day and night	Solar-driven water release	Arizona Desert: 0.1 L kg_{MOF}^{-1}	[53]
MIL-101(Cr)	Coating on a copper foam	Stable operation for a continuous week	Solar-driven water release coupled with thermoelectric power generation	Outdoor: 0.93 L kg_{MOF}^{-1} [b]	[185]
LiCl@MIL-101(Cr)	Powder bed	Stable operation for a day and night	Solar-driven water release	Outdoor: 0.45 L kg_{MOF}^{-1}	[81]
COF-ok[a]	Powder bed	Stable operation for a day and night	Solar-driven water release	Indoor: 0.212 L kg_{COF}^{-1} Outdoor: 0.161 L kg_{COF}^{-1}	[91]
AQSOA-Z01[a]	Infiltrated into the nickel foam	Stable operation for a day and night	Dual-stage AAWH with solar-driven water release	Outdoor: 0.115 L $kg_{sorbent}^{-1}$ [c]	[189]
MXene Ti_3C_2/UiO-66(Zr)-NH_2/SA	Monolith	Stable operation for 9 h	Flippable adsorbent stage with solar-driven water release	Indoor: 0.058 L h^{-1} kg_{MOF}^{-1} (productivity per hour)	[26]
Active multicyclic AAWH device					
MIL-101(Cr)/SA (MF@MIL-1)	MOF/SA (sodium alginate) monolith with Metal foam (MF) embedded	Stable operation for 24 h (continuous 8 water harvesting cycles, 3 h each cycle)	Localized eddy current heating (LECH) triggered water release	Indoor: 2.2 L kg_{MOF}^{-1}	[25]
Al-fumarate/SA	MOF/SA monolith with cylindrical carbon fiber (CF) bundle embedded	Stable operation for 24 h (continuous 7.2 water harvesting cycles)	Localized electrical heating (LEH) triggered water release	Indoor: 1.7 L kg_{MOF}^{-1} Outdoor: 1.2 L kg_{MOF}^{-1}	[135]
MOF-303(Al)	Powder bed	Stable operation for 3 days	Solar-powered electric heating triggered water release	Indoor: 1.3 L kg_{MOF}^{-1} Mojave Desert: 0.7 L kg_{MOF}^{-1}	[182]
MOF-801(Zr)	Fluidization of powder	Stable operation for 10 water harvesting cycles (36 min per cycle at 18% RH, 26 min per cycle at 39% RH)	Electric heated hot flow triggered water release	18% RH: 0.33 L h^{-1} kg_{MOF}^{-1} 39% RH: 0.52 L h^{-1} kg_{MOF}^{-1} (productivity per hour)	[190]
Al-fumarate/CNTs/SA	MOF/CNTs (carbon nanotubes)/SA monolith with a carbon paper embedded in the middle	Stable operation for 3 days	Solar-driven (daytime) and electric heating (night) triggered water release	Indoor: 1.4 L kg_{MOF}^{-1}	[28]
Al-fumarate/CS/SA (CAS)	MOF/SA monolith with a carbon scaffold (CS) embedded	Stable operation for 22.5 h (continuous 9 water harvesting cycles, 2.5 h each cycle)	Localized electrical heating (LEH) triggered water release	Indoor: 1.95 L kg_{CAS}^{-1}	[24]
Adaptive multicyclic AAWH device					
MOF-801(Zr)	MOF powder on parallel aluminon-lined trays	Stable operation over month > 1000 cycles in Amman desert	Electrical heating desorption air Refrigeration-compressor cooling	Indoor: 1.2–2.4[d] 1.8–3.5[d] L kg_{MOF}^{-1}	[132]

[a] AQSOA-Z01 and COF-ok are benchmarks for comparison; [b] Converted from the numerical values reported in the literature: Copper foam of 0.1 × 0.1 m^2 with 8.1 g_{MOF} and 7.5 g working capacity; [c] Converted from the numerical values reported in the literature: Nickel foams loaded with 305 g and 215 g AQSOA-Z01 in total and about 60 mL collected water; [d] 10–30% RH and 30–60% RH, respectively. Power consumption 1.67–5.25 and 3–7 kWh L^{-1}, respectively, conditions dependent. No info given on particle size or shape used.

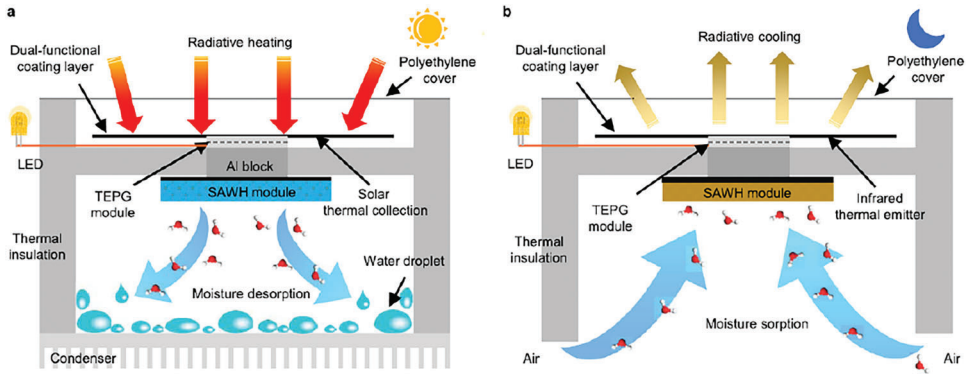

Figure 16. The passive monocyclic AAWH device coupled with 24 h thermoelectric power generation (TEPG). Reproduced with permission.[185] Copyright 2022, Springer Nature.

thermal radiation from the sun. The released vapor is concentrated and then condensed. It has been proven that the passive monocyclic AAWH device when using MOFs as adsorbents, is able to generate drinking water with little (theoretically no) external energy sources.[131,183]

The MOF-801(Zr) based device exhibited an average productivity of 0.1 L kg_{MOF}^{-1} of water a day in Arizona Desert.[53] Other passive monocyclic AAWH devices also showed similar productivity levels (Table 5), which are by far not enough to meet the daily needs of an adult (at least 4 L per day).[184] However, by ingenious coupling passive monocyclic AAWH, based on MIL-101(Cr) coated on a copper foam plate, and 24 h thermoelectric power generation (TEPG), not only the all-day thermoelectric power density can be improved (≈346%), but also the stationary water production can be improved nearly ten times (0.93 L kg_{MOF}^{-1} per day) (**Figure 16**).[185] Crucial in improving the daily water production of the passive monocyclic AAWH device is a MOF with high water adsorption capacity at low humidity, but which usually requires a higher regeneration temperature. Feng et al. analyzed in detail this dilemma considering the (ideal) thermal efficiency of a sorbent, showing the much higher thermal efficiency of a sorbent with a step at higher RH, which is incompatible with use in arid climates.[184] Cooling-assisted sorption-enhanced atmospheric water harvesting (CSAWH) may alleviate this issue. Using a cooling source the effective RH near the sorbent is increased and such sorbent can be used competitively with one adsorbing at lower RH, despite extra cooling demands and low solar-to-electricity efficiency.

An "active" multicyclic AAWH device can realize multiple water collection cycles per day through the multiple adsorption–desorption cycles of the adsorbent, which breaks the limit of the water adsorption capacity of the adsorbent in the passive monocyclic AAWH device. A MOF-303(Al)-based active multicyclic AAWH device (≈1.3 L kg_{MOF}^{-1} per day)[182] exhibited an increased productivity compared with the passive monocyclic MOF-801(Zr)-based device reported by the same team (≈0.1 L kg_{MOF}^{-1} per day).[53] The MOF adsorbent requires active mild heating to release the adsorbed water vapor to realize uptake and release cycling during day and night. As summarized in Table 5, electric and/or solar heating are used as active mild heating. Compared with the passive monocyclic device, the productivity of the active multicyclic AAWH device has been improved by an order of magnitude. Bezrukov et al. optimized the uptake-release cycle time of several MOFs. Using only partially the working capacity by faster cycling the overall productivity can be increased. Assuming a thermal swing operation between 27 °C @ 30% RH and 60 °C @ 5.4% RH can be realized and using ROS-039/cellulose paper composite (ROS-039 = [Zn(1,2,4-triazole)F]n), a projected productivity of 7.3 L kg_{MOF}^{-1} per day is obtained, sufficient for a daily need.[19] Although not explored in this composite form, their data suggest even better performances for MOF-303 and MIL-160. Applying CSAWH in multicyclic operation using sorbents with a step at higher RH also have the prospect to yield larger productivity.[184]

An "adaptive" water harvesting device was recently reported by Almassad et al. using aluminum-coated trays with MOF-801.[132] Compared to an "active" device with a fixed adsorption-desorption cycle, the water harvesting cycle was real-time adapted depending on the weather/seasonal conditions. Depending on the applied conditions (10–30% RH) the water production of the active device was improved from 1.2 to 2.4 L kg_{MOF}^{-1} per day for the adaptive device and even further doubled for 30–60% RH conditions. Interestingly, in a cost analysis for 100 devices with 1 kg MOF based on this system, a projected drinking water cost for Jordan is forecasted to range from 0.064 $ (off-grid) to 0.167–0.525 $ (on-grid).

Most examples of AWH refer to a discontinuous operation of the uptake-release cycle, but a few examples explore a continuous operation based on a rotating wheel.[186,187]

To date, MOF-based AAWH has attracted increasingly more attention, and highly interesting daily water production levels are reported, but a commercial MOF-based device has not yet been reported, unlike the "Hydropanel" based on classical sorbents.[188] Further effort should be focused on practical applications with MOFs. The large-scale production of MOF materials is the first step toward industrialization of MOF-based AAWH. It is great to see the production of kilogram-scale high-performance MOFs (as shown in Table 2). However, when for practical use the MOF powder is shaped into bodies, fabrics, or coatings, capacity loss due to binder use or performance degradation[146] may inevitably occur. This underexposed aspect in formulation requires attention. It should be kept in mind that in the multicyclic operation, stricter requirements for the hydrothermal stability and recyclability of MOFs apply.

Reducing heat loss, performing heat recovery, and addressing the heat and mass transportation issues during active cycling are the next aspects that require an integral approach toward device realization. Example directions given include the use of structured heat conducting composites, radiative cooling, cooling-assisted sorption, optimizing the harvesting cycle by partially utilizing the working capacity, and adapting the harvesting cycle based on the monitoring of the weather or seasonal variations.

5.3.2. Desalination

Opposite to the water harvesting in arid areas, water production by desalination from brackish and seawater is commercially well applied.[191,192] An emerging technology is adsorption desalination (AD).[113] The principle is similar to that of a heat pump, but now as an open system where the condensed water is the targeted product while the cooling performance is second.[5] In our previous review demonstration units in Singapore and at KAUST employing silica gel were reported,[113,193] while hardly work with MOFs was available.[194,195] Key performance indicator (KPI) is the specific daily water production (SDWP). In cogeneration, the specific cooling power (SCP) is another important KPI. As a reference for silica, SDWP values range up to 10 $m^3 tonne^{-1}_{silica}\ day^{-1}$ for a dual bed system, a PR ≈0.75, and SCP up to 100 $W\ kg^{-1}_{silica}$.[193] Only MIL-101(Cr), Al-fumarate and CPO-27Ni were compared for a two-bed system with SDWP values up to 11, 6.3 and 4.6 $m^3 tonne^{-1}_{MOF}\ day^{-1}$, respectively, but at a high regeneration temperature of 150 °C (required for CPO-27 regeneration).[195] Note that the water has generally the quality of deionized water.

Numerical modeling confirmed the promising performance of Al-fumarate.[118] KPI values strongly depend on the operation parameters. Similarly, Wang et al. compared twelve different sorbents.[196] The MOFs MIL-100(Fe), DUT-67, Al-fumarate, UiO-66, and MIL-101(Cr) outperformed other sorbents and, depending on the applied conditions, their SDWP surpassed 10 $m^3 tonne^{-1}_{MOF}\ day^{-1}$. Youssef et al. also investigated experimentally the performance of 0.67 kg CPO-27(Ni) packing in a single bed desalinator.[194] At optimal conditions (regeneration at 95 °C) the SDWP could reach 22.8 $m^3 tonne^{-1}_{MOF}\ day^{-1}$, and SCP up to 750 $W\ kg^{-1}_{MOF}$.

Recently, Elsayed et al. demonstrated in a labscale dual packed bed heat exchanger for Al-fumarate (0.375 kg each) improved KPIs for regeneration at 90 °C with SDWP up to 12.7 $m^3 tonne^{-1}_{MOF}\ day^{-1}$, and SCP up to 318 $W\ kg^{-1}_{MOF}$, decreasing with increasing cooling temperature,[197] an important improvement over their results for silica gel and CPO-27. Coating instead the fins of the heat exchanger tubes with Al-fumarate and using hydroxyethyl cellulose binder doubled the SDWP to 23.5 $m^3 tonne^{-1}_{MOF}\ day^{-1}$ with an SCP of 682 $W\ kg^{-1}_{MOF}$.[154] The COF of 0.32 is modest in this cogeneration system, but still higher than in the packed system.

Han et al. considered various functionalized UiO(Zr) MOFs numerically for modeling desalination.[198] Compared to the parent MOF functionalization increased the SDWP from 24 to 40 $m^3 tonne^{-1}_{MOF}\ day^{-1}$ and the SCP from 360 to 840 $W\ kg^{-1}_{MOF}$.

These recent studies, using MOFs for AD indicate large improvements over the commercially used silica gel reference, and hold promises for practical application provided the large-scale availability of the MOFs and at an acceptable price.

5.4. Other Applications

As mentioned earlier in this paper, in principle MOFs can be applied in most applications where control of humidity is required, or adsorption-based heating or cooling is utilized. A selection of specific examples where MOFs play or could play a role are given here.

5.4.1. Thermal-to-Mechanical Energy Conversion

Water sorption can be transformed into mechanical energy. A superhydrophobic flexible nanoporous MOF, Cu_2(tebpz),[199] possesses the ability to realize a reversible nonhysteretic wetting (contraction) – drying (expansion) cycle induced by periodic temperature fluctuations and displays a thermal to mechanical conversion efficiency of about 30%. It offers a possibility that hydrophobic flexible nanoporous MOFs, in interaction with water, can be used for compact energy conversion.

5.4.2. Enhanced Proton Conductivity

Adsorbed H_2O plays an important role in proton conductive MOFs,[200–203] which means that a MOF with stronger water retention ability can exhibit better proton conductivity. A Cu-based MOF (CuCpz) has been verified to be able to sustain an excellent water uptake capacity from 100% to 43% RH, and thus maintain its enhanced proton conductivity over a wide RH range.[204]

5.4.3. Humidity Sensing

The application of MOFs in humidity sensing is noteworthy.[205] The film, which is assembled by aggregation-induced-emission luminogen (AIEgen)-based MOF nanosheets and seaweed cellulose nanofibrils, shows reversible changes in fluorescence emission intensity in response to ambient humidity between 50% and 100% RH, which can be used for humidity sensing.[206]

5.4.4. Passive Thermal Management

Battery thermal management is critical in safe, fast charging and discharging. Xu et al. propose a self-adaptive SBTM (smart battery thermal management) device based on MIL-101(Cr)@carbon foam coating of a Li-ion battery.[207] At low temperature air humidity will adsorb, warming up slightly this coating. At high temperatures thermal dissipation by desorption will provide a cooling effect. The heat is well dissipated through the excellent heat conduction of the carbon foam. The ambient operating conditions of MOFs are perfect for this device, and even an optimal selection can be made depending on the regional conditions. The self-regeneration of the MOF results in a nearly zero

energy self-adaptive smart thermal management. In principle, this idea can be applied much wider to more electronic devices requiring cooling. Photovoltaic panels can be cooled by water evaporation from a MOF thermal battery during daytime increasing their electricity generation by 5%. The MOF battery adsorbs water vapor during the night.[208] This can even be combined with humidity control in the building.

5.4.5. Comfortable Clothing

By spray electrospinning MIL-101(Cr) containing nanofibrous flexible composite tissue was obtained with excellent uptake kinetics. This fabric can be used for improving the wet-thermal comfort of clothing, absorbing an excess of sweat.[20]

5.4.6. Humidor

Cigars must be stored under well-controlled humidities of ≈65–75% RH to preserve their quality. Special boxes for this purpose are called humidors, actively controlling the internal humidity. A low-cost solution for traveling could be a box containing a certain amount of MOF exhibiting the adsorption-desorption step in the optimal RH region, like PIZOF-2.[37] The interior humidity is then controlled passively. Alternative candidates could be MIL-101(Cr) or BIT-66(V), but probably other systems exist that are kept unreported because of the strong focus on lower RH ranges.

5.4.7. Dishwasher

Siemens/Bosch introduced a home appliance dishwasher[209,210] equipped with an open adsorption system based on the work of Hauer and Fischer using a zeolite 13X packed bed.[211] The drying of the dishes is done by dry hot air generated by the heat of water adsorption. Regeneration takes place by heating during the next washing cycle. Energy consumption was reduced by 25%. Using low-cost Siogel (≈5 € kg^{-1}), selected in a comparative study,[212] a 41% reduction was obtained. Bardow et al., benchmarking commercial sorbents, showed that using commercial silica gel (SG127B) also the amount of sorbent could be reduced by 50%, also drying time was reduced.[213,214] An evaluation of thermal performance of MOF sorbents as an alternative for this application would be interesting. The cost of MOFs will be higher, but not prohibitive in view of the amount needed (<1 kg).[212,213]

5.4.8. Washer Dryer

Cranston et al. analyzed the implementation of a sorption bed in a heat pump-based washer-dryer.[215] The sorption bed creates a lower humidity of the drying air, so a larger driving force for drying clothes. Without regeneration of the silica-supported ionic liquid composite sorbent, the energy efficiency was improved by 18%, and the drying time was shortened by 19 min to 85 min. Including sorbent regeneration the energy efficiency was only 7% improved and drying took 98 min. The performance of MOFs through their steep adsorption step and easy regeneration is worth further analysis.

6. Evaluative Remarks–Outlook

In current modern society humidity and temperature control are indispensable in daily life and commercial activities. Utilizing the heat effects of water evaporation or condensation is often based on primary energy sources resulting in the undesired associated CO_2 emission. From the viewpoint of sustainability utilization of renewable (solar, wind) or low-grade "waste" heat sources are highly desirable.

The special class of crystalline porous materials, MOFs and COFs, possesses attractive properties for application in the abovementioned activities, contributing to the reduction of primary energy consumption and CO_2 footprint. They stand out over classical porous materials, including zeolites, due to their step-like water adsorption isotherm and easy regeneration over a small temperature or vapor pressure window. In principle, MOFs can be applied in most applications where water vapor control is used for heat reallocation and humidity control.

In this review update, a few dozen MOFs are identified that comply with the required properties of step-isotherm with easy regeneration, reasonable working capacity, hydrothermal stability, and cyclic durability. Several synthesis methods can be used to further improve or fine-tune these properties (including step location and steepness) among which the systematic approaches of polymorphism[11] and multivariate[77,181] synthesis seem most promising. They both focus on controlling the way AlO_6 octahedral building blocks are coupled in the linear inorganic chains of Al-MOFs. The former deals with controlling the pure *cis*, *trans*, or mixed *cis-trans* coupling of the AlO_6 octahedra through different single organic linkers, the latter uses mixtures of linkers, affecting the coupling of the AlO_6 octahedra.

In the literature various illustrations of the use and stability of MOFs in applications under cyclic operation can be found, indicating their potential. However, the availability of sufficient quantities of material and the cost aspect are becoming crucial for real-life demonstration and market penetration of a specific application. In principle, the batch-wise lab synthesis can be scaled up to a certain extent,[88,106] but for large-scale applications, like energy storage, heat pumps, and desalination, large quantities must be available. Continuous synthesis technologies can constitute a breakthrough with easier operation and quality control. Production cost may also come down, essential in the comparison with (the price of) existing used sorbents. Although not excessively, in some publications the cost of MOF production is estimated, although the cost bases differ.[101,106,216–218] Important is the complete techno-economic analysis (TEA) and life cycle analysis (LCA) of the whole synthesis from feedstock to products.[216,,217] In most studies the predicted large-scale production costs fall below ≈10 € kg^{-1}.[216,218] Important cost contribution is that of the linker and large-scale production may considerably help cost reduction, as can be expected for furan dicarboxylic acid for MIL-160(Al). This material is 100% plant-based, made from sugars and even cellulose, and is used as feedstock for PEF bottles, the green alternative for PET.[219]

Most synthetic MOF literature focuses on working capacity and tuning the inflection point of water uptake. But next to an optimal MOF, each application needs the right morphology of the MOF to combine and optimize the opposite requirements of fast heat (dense, conductive material) and

Table 6. Indicative technology readiness levels (TRL)[231] of selected technologies or products based on water adsorption using MOFs.

Development Phase	TRLS	Application	TRL	References
DISCOVERY	1–3	Thermal-to-mechanical energy conversion	1	[199]
		Enhanced proton conductivity	1	[204]
		Comfortable clothing	3	[20]
		Humidity sensing	3	[206]
DEVELOPMENT	4–6	Passive thermal management	4	[207,208]
		Washer Dryer	5	[215]
		Humidity control (DAC)	4 (8*)	[148,150] ([235–237]*)
		Desalination	6 (8*)	[194,197] ([113,193]*)
		Adsorption chiller	6 (9*)	[101,156,221] ([114,162,238]*)
DEMONSTRATION	7–8	Water harvesting	7 (8*)	[131,132,182,239] ([188]*)
DEPLOYMENT	9	Dishwasher	(9*)	([209,210,212,213]*)

*Values with asterisk apply to the use of other sorbents.

water vapor (porous structure) transport, on various levels, from MOF to the full device.[5,18] This transport determines the cycle times for loading and unloading, an important design parameter for optimization.[220,221] Shaping MOF powder into particles for packed bed operation, coating of heat exchange surfaces, or thermoconductive supports requires dedicated formulation technologies, often based on specific binder materials. The detailed determination of kinetics properties of MOFs, composites, and full devices, essential for the engineering modeling of the system performance, is an underexplored area.[12,14„18,24,25,82,115,120,124,146,222–227]

Various examples of small to large-scale applications of MOFs utilizing their water adsorption-desorption and associated enthalpy changes have been described in the preceding paragraph, in earlier reviews, and other potential applications are highlighted. Very interesting is the application of MOF composites in self-adaptive passive thermal management for electric devices.[207,208] It must be clear that there is no one-MOF-fits-all. Each application requires specific operation conditions that may even depend on the regional location, and hence only some specific MOFs will qualify. This accounts for the various candidates listed in Table 1 and Figures 5 and 7(a). Apart from experimental selection, evaluation through high-throughput computational screening may offer an interesting exploration of high-performing adsorbents.[228] In cascaded adsorption heat pumps[229,230] an optimal combination of a COF in the low-temperature stage and a MOF in the high-temperature stage was identified (although using a higher regeneration temperature of 400 K). Here, a dominant role of a high working capacity and a moderate adsorption enthalpy was identified yielding an overall $COP_C > 1.6$.[228]

To indicate the maturity of some MOF applications we estimated the technology readiness level (TRL, see supporting info[231]) based on published literature (**Table 6**). In some cases, the use of classical sorbents is already at a more advanced level than the MOF application, but the special characteristics of MOFs hold potential. Regarding such practical evaluation, retrofitting with MOFs existing processes based on classical desiccants or sorbents, like in air conditioning,[165] desalination[113,154,193,198] and adsorption-based heat pumps,[162,232] may provide a relatively rapid assessment of applicability. However, TRL only measures technology maturity. For realization of large-scale applications feasibility studies should be made through techno-economic analyses (TEA) in which within specified battery limits the investment and operating costs (CAPEX and OPEX) are evaluated in comparison with existing competitive systems.[111–114,217,218,233] Including sensitivity analyses of MOF type, cost, working capacity, and energy utilization (renewable/waste) will provide insight into which MOF and system layout to be used, and guides directions for further optimization development. TEA can even point at the use of a MOF that would not necessarily be the first choice based on adsorption characteristics. Life Cycle Assessment (LCA) analysis may provide further arguments for acceptability of such an application, the used MOF, and the CO_2 footprint.[216,234]

In summary, an update is presented on the status of development of MOFs as dedicated water sorbents in heat reallocation, water harvesting, and humidity control. An outlook is given on necessary steps forward for realizing their practical implementation, addressing the societal challenges in reducing primary energy consumption by utilizing waste and solar heating.

After emphasizing some essential basic aspects, this review covers whole range from MOF synthesis to application, thermodynamics to engineering. Taking the steep water uptake in the isotherm as the most important of six criteria, ≈40 MOFs and one COF are selected, each suited for a different specific application, as no single MOF-fits-all. Two interesting synthesis approaches for further MOF optimization are identified, based on polymorphism and multivariate synthesis. Selected applications are described in more detail with emphasis on dehumidification, air conditioning, water harvesting, and desalination, while several potential other cases are highlighted.

For modeling, optimization, and cycle control, kinetics of the mass and heat transport in adsorption-based applications require further exploration. A rapid breakthrough is expected by retrofitting existing set-ups based on classical sorbents with MOFs. Finally, techno-economic analysis combined with life cycle analysis, both for synthesis scale-up and full-scale applications, are essential to demonstrate their feasibility and social and commercial acceptance.

Supporting Information

Supporting Information is available from the Wiley Online Library or from the author.

Acknowledgements

This work was financially supported by the National Key Research and Development Program (2021YFB3801200), the National Natural Science Foundation of China (22008171, 22178164, 21908097), Jiangsu Specially-Appointed Professors Program and State Key Laboratory of Materials-Oriented Chemical Engineering (ZK202002).

Conflict of Interest

The authors declare no conflict of interest.

Keywords

adsorption desalination, humidity control, MOF formulation, water adsorption isotherm, water harvesting

Received: April 30, 2023
Revised: July 5, 2023
Published online:

[1] M. Thommes, K. Kaneko, A. V. Neimark, J. P. Olivier, F. Rodriguez-Reinoso, J. Rouquerol, K. S. W. Sing, *Pure Appl. Chem.* **2015**, *87*, 1051.
[2] S. Kitagawa, R. Kitaura, S.-i. Noro, *Angew. Chem., Int. Ed.* **2004**, *43*, 2334.
[3] J. L. C. Rowsell, O. M. Yaghi, *Microporous Mesoporous Mater.* **2004**, *73*, 3.
[4] N. Hanikel, X. K. Pei, S. Chheda, H. Lyu, W. Jeong, J. Sauer, L. Gagliardi, O. M. Yaghi, *Science* **2021**, *374*, 454.
[5] X. Liu, X. Wang, F. Kapteijn, *Chem. Rev.* **2020**, *120*, 8303.
[6] M. F. de Lange, K. J. F. M. Verouden, T. J. H. Vlugt, J. Gascon, F. Kapteijn, *Chem. Rev.* **2015**, *115*, 12205.
[7] L. G. Gordeeva, Y. D. Tu, Q. Pan, M. L. Palash, B. B. Saha, Y. I. Aristov, R. Z. Wang, *Nano Energy* **2021**, *84*, 105946.
[8] S. K. Henninger, F. Jeremias, H. Kummer, C. Janiak, *Eur. J. Inorg. Chem.* **2012**, *2012*, 2625.
[9] R. M. Felder, R. W. Rousseau, *Elementary principles of chemical processes*, Wiley, New York, **2005**.
[10] D. Ma, P. Li, X. Duan, J. Li, P. Shao, Z. Lang, L. Bao, Y. Zhang, Z. Lin, B. Wang, *Angew. Chem., Int. Ed.* **2020**, *59*, 3905.
[11] T. J. Matemb Ma Ntep, M. Wahiduzzaman, E. Laurenz, I. Cornu, G. Mouchaham, I. Dovgaliuk, S. Nandi, K. Knop, C. Jansen, F. Nouar, P. Florian, G. Fuldner, G. Maurin, C. Janiak, C. Serre, *Adv. Mater.* **2023**, 2211302.
[12] C. Sun, Y. Zhu, P. Shao, L. Chen, X. Huang, S. Zhao, D. Ma, X. Jing, B. Wang, X. Feng, *Angew. Chem., Int. Ed.* **2023**, *62*, 202217103.
[13] M. F. de Lange, T. Zeng, T. J. H. Vlugt, J. Gascon, F. Kapteijn, *CrystEngComm* **2015**, *17*, 5911.
[14] S. Graf, F. Redder, U. Bau, M. de Lange, F. Kapteijn, A. Bardow, *Energy Technol.* **2020**, *8*, 1900617.
[15] E. Alvares, S. Tantoro, C. Julius, K. C. Cheng, F. E. Soetaredjo, H. Y. Hsu, A. E. Angkawijava, A. W. Go, C. W. Hsieh, S. P. Santoso, *Int. J. Biol. Macromol.* **2023**, *231*, 123322.
[16] L. Wang, P. Chen, X. Dong, W. Zhang, S. Zhao, S. Xiao, Y. Ouyang, *RSC Adv.* **2020**, *10*, 44679.
[17] J. Troyano, C. Camur, L. Garzon-Tovar, A. Carne-Sanchez, I. Imaz, D. Maspoch, *Acc. Chem. Res.* **2020**, *53*, 1206.
[18] D. Farrusseng, C. Daniel, C. Hamill, J. Casaban, T. Didriksen, R. Blom, A. Velte, G. Fueldner, P. Gantenbein, P. Persdorf, X. Daguenet-Frick, F. Meunier, *Faraday Discuss.* **2021**, *225*, 384.
[19] A. A. Bezrukov, D. J. O'Hearn, V. Gascon-Perez, S. Darwish, A. Kumar, S. Sanda, N. Kumar, K. Francis, M. J. Zaworotko, *Cell Rep. Phys. Sci.* **2023**, *4*, 101252.
[20] A. L. Li, J. Xiong, Y. Liu, L. M. Wang, X. H. Qin, J. Y. Yu, *Energy Environ. Mater.* **2023**, *6*, 12254.
[21] X. Liu, P. Li, J. Chen, P. Jiang, Y.-W. Mai, X. Huang, *Sci. Bull.* **2022**, *67*, 1991.
[22] H. Lee, H. Lee, S. Ahn, J. Kim, *ACS Omega* **2022**, *7*, 21145.
[23] A. Karmakar, V. Prabakaran, D. Zhao, K. J. Chua, *Appl. Energy* **2020**, *269*, 115070.
[24] Y. Tao, Q. Wu, C. Huang, D. Zhu, H. Li, *Chem. Eng. J.* **2023**, *451*, 138547.
[25] Y. Tao, Q. Li, Q. Wu, H. Li, *Mater. Horiz.* **2021**, *8*, 1439.
[26] Q. N. Wu, W. Su, Q. Q. Li, Y. L. Tao, H. Q. Li, *ACS Appl. Mater. Interfaces* **2021**, *13*, 38906.
[27] W. Su, Y. Tao, Q. Wu, H. Li, *ACS Appl. Mater. Interfaces* **2022**, *14*, 39637.
[28] Y. Tao, Q. Wu, C. Huang, W. Su, Y. Ying, D. Zhu, H. Li, *ACS Appl. Mater. Interfaces* **2022**, *14*, 10966.
[29] M. Ambrosetti, G. Groppi, W. Schwieger, E. Tronconi, H. Freund, *Chem. Eng. Process.* **2020**, *155*, 108057.
[30] S. Zhang, J. Fu, G. Xing, W. Zhu, T. Ben, *Chem. Synth.* **2023**, *3*, 10.
[31] K. Wu, Z. Chen, J. Li, X. Li, J. Xu, X. Dong, *Proc. Natl. Acad. Sci. U.S.A.* **2017**, *114*, 3358.
[32] M. F. De Lange, J.-J. Gutierrez-Sevillano, S. Hamad, T. J. H. Vlugt, S. Calero, J. Gascon, F. Kapteijn, *J. Phys. Chem. C* **2013**, *117*, 7613.
[33] J. Canivet, A. Fateeva, Y. Guo, B. Coasne, D. Farrusseng, *Chem. Soc. Rev.* **2014**, *43*, 5594.
[34] J. Canivet, J. Bonnefoy, C. Daniel, A. Legrand, B. Coasne, D. Farrusseng, *New J. Chem.* **2014**, *38*, 3102.
[35] S. M. T. Abtab, D. Alezi, P. M. Bhatt, A. Shkurenko, Y. Belmabkhout, H. Aggarwal, L. J. Weselinski, N. Alsadun, U. Samin, M. N. Hedhili, M. Eddaoudi, *Chem* **2018**, *4*, 94.
[36] D. D. Do, S. Junpirom, H. D. Do, *Carbon* **2009**, *47*, 1466.
[37] H. Furukawa, F. Gandara, Y.-B. Zhang, J. Jiang, W. L. Queen, M. R. Hudson, O. M. Yaghi, *J. Am. Chem. Soc.* **2014**, *136*, 4369.
[38] M. A. van der Veen, S. Canossa, M. Wahiduzzaman, G. Nenert, D. Frohlich, D. Rega, H. Reinsch, L. Shupletsov, K. Markey, D. E. De Vos, M. Bonn, N. Stock, G. Maurin, E. H. G. Backus, *Adv. Mater.* **2023**, 2210050.
[39] H. L. Nguyen, N. Hanikel, S. J. Lyle, C. Zhu, D. M. Proserpio, O. M. Yaghi, *J. Am. Chem. Soc.* **2020**, *142*, 2218.
[40] A. J. Rieth, A. M. Wright, S. Rao, H. Kim, A. D. LaPotin, E. N. Wang, M. Dincă, *J. Am. Chem. Soc.* **2018**, *140*, 17591.
[41] M. J. Kalmutzki, C. S. Diercks, O. M. Yaghi, *Adv. Mater.* **2018**, *30*, 1704304.
[42] A. J. Rieth, S. Yang, E. N. Wang, M. Dinca, *ACS Cent. Sci.* **2017**, *3*, 668.
[43] M. Wahiduzzaman, D. Lenzen, G. Maurin, N. Stock, M. T. Wharmby, *Eur. J. Inorg. Chem.* **2018**, *32*, 3626.
[44] N. Ko, J. Hong, S. Sung, K. E. Cordova, H. J. Park, J. K. Yang, J. Kim, *Dalton Trans.* **2015**, *44*, 2047.
[45] G. Ferey, C. Mellot-Draznieks, C. Serre, F. Millange, J. Dutour, S. Surble, I. Margiolaki, *Science* **2005**, *309*, 2040.
[46] P. Kuesgens, M. Rose, I. Senkovska, H. Froede, A. Henschel, S. Siegle, S. Kaskel, *Microporous Mesoporous Mater.* **2009**, *120*, 325.
[47] A. J. Rieth, A. M. Wright, G. Skorupskii, J. L. Mancuso, C. H. Hendon, M. Dinca, *J. Am. Chem. Soc.* **2019**, *141*, 13858.
[48] S. Bagi, A. M. Wright, J. Oppenheim, M. Dinca, Y. Roman-Leshkov, *ACS Sustainable Chem. Eng.* **2021**, *9*, 3996.

[49] E. Alvarez, N. Guillou, C. Martineau, B. Bueken, B. Van de Voorde, C. Le Guillouzer, P. Fabry, F. Nouar, F. Taulelle, D. de Vos, J.-S. Chang, K. H. Cho, N. Ramsahye, T. Devic, M. Daturi, G. Maurin, C. Serre, *Angew. Chem., Int. Ed.* **2015**, *54*, 3664.
[50] H. Reinsch, M. A. van der Veen, B. Gil, B. Marszalek, T. Verbiest, D. de Vos, N. Stock, *Chem. Mater.* **2013**, *25*, 17.
[51] A. Cadiau, J. S. Lee, D. D. Borges, P. Fabry, T. Devic, M. T. Wharmby, C. Martineau, D. Foucher, F. Taulelle, C.-H. Jun, Y. K. Hwang, N. Stock, M. F. De Lange, F. Kapteijn, J. Gascon, G. Maurin, J.-S. Chang, C. Serre, *Adv. Mater.* **2015**, *27*, 4775.
[52] D. Lenzen, J. Zhao, S.-J. Ernst, M. Wahiduzzaman, A. K. Inge, D. Froehlich, H. Xu, H.-J. Bart, C. Janiak, S. Henninger, G. Maurin, X. Zou, N. Stock, *Nat. Commun.* **2019**, *10*, 3025.
[53] F. Fathieh, M. J. Kalmutzki, E. A. Kapustin, P. J. Waller, J. Yang, O. M. Yaghi, *Sci. Adv.* **2018**, *4*, eaat3198.
[54] K. H. Cho, D. D. Borges, U. H. Lee, J. S. Lee, J. W. Yoon, S. J. Cho, J. Park, W. Lombardo, D. Moon, A. Sapienza, G. Maurin, J. S. Chang, *Nat. Commun.* **2020**, *11*, 5112.
[55] N. Hanikel, D. Kurandina, S. Chheda, Z. Zheng, Z. Rong, S. E. Neumann, J. Sauer, J. I. Siepmann, L. Gagliardi, O. M. Yaghi, *ACS Cent. Sci.* **2023**, *3*, 551.
[56] J. Li, Y. Wang, Y. Chen, Q. Xiong, J. Yang, L. Li, J. Li, *Chin. J. Chem. Eng.* **2022**, *49*, 170.
[57] A. Cadiau, Y. Belmabkhout, K. Adil, P. M. Bhatt, R. S. Pillai, A. Shkurenko, C. Martineau-Corcos, G. Maurin, M. Eddaoudi, *Science* **2017**, *356*, 731.
[58] R. G. AbdulHalim, P. M. Bhatt, Y. Belmabkhout, A. Shkurenko, K. Adil, L. J. Barbour, M. Eddaoudi, *J. Am. Chem. Soc.* **2017**, *139*, 10715.
[59] Z. J. Chen, P. H. Li, X. Zhang, P. Li, M. C. Wasson, T. Islamoglu, J. F. Stoddart, O. K. Farha, *J. Am. Chem. Soc.* **2019**, *141*, 2900.
[60] A. D. Wiersum, E. Soubeyrand-Lenoir, Q. Yang, B. Moulin, V. Guillerm, M. Ben Yahia, S. Bourrelly, A. Vimont, S. Miller, C. Vagner, M. Daturi, G. Clet, C. Serre, G. Maurin, P. L. Llewellyn, *Chem. Asian J.* **2011**, *6*, 3270.
[61] X. Liu, N. K. Demir, Z. Wu, K. Li, *J. Am. Chem. Soc.* **2015**, *137*, 6999.
[62] J. H. Cavka, S. Jakobsen, U. Olsbye, N. Guillou, C. Lamberti, S. Bordiga, K. P. Lillerud, *J. Am. Chem. Soc.* **2008**, *130*, 13850.
[63] S. Wang, J. S. Lee, M. Wahiduzzaman, J. Park, M. Muschi, C. Martineau-Corcos, A. Tissot, K. H. Cho, J. Marrot, W. Shepard, G. Maurin, J.-S. Chang, C. Serre, *Nat. Energy* **2018**, *3*, 985.
[64] J. S. Lee, J. W. Yoon, P. G. M. Mileo, K. H. Cho, J. Park, K. Kim, H. Kim, M. F. de Lange, F. Kayteijn, G. Maurin, S. M. Humphrey, J.-S. Chang, *ACS Appl. Mater. Interfaces* **2019**, *11*, 25778.
[65] Y. Chen, Y. D. Du, Y. Wang, R. Krishna, L. B. Li, J. F. Yang, J. P. Li, B. Mu, *AIChE J.* **2021**, *67*, 17152.
[66] X. Tang, Y. Luo, Z. Zhang, W. Ding, D. Liu, J. Wang, L. Guo, M. Wen, *Chem. Phys.* **2021**, *543*, 111093.
[67] A. Shigematsu, T. Yamada, H. Kitagawa, *J. Am. Chem. Soc.* **2011**, *133*, 2034.
[68] J. W. Zhang, P. Li, X. N. Zhang, X. J. Ma, B. Wang, *ACS Appl. Mater. Interfaces* **2020**, *12*, 46057.
[69] B. Li, F. F. Lu, X. W. Gu, K. Shao, E. Wu, G. Qian, *Adv. Sci.* **2022**, *9*, 2105556.
[70] F.-F. Lu, X.-W. Gu, E. Wu, B. Li, G. Qian, *J. Mater. Chem. A* **2023**, *11*, 1246.
[71] N. X. Zhu, Z. W. Wei, C. X. Chen, X. H. Xiong, Y. Y. Xiong, Z. Zeng, W. Wang, J. J. Jiang, Y. N. Fan, C. Y. Su, *Angew. Chem., Int. Ed.* **2022**, *61*, 7.
[72] Z. Lu, J. Duan, H. Tan, L. Du, X. Zhao, R. Wang, S. Kato, S. Yang, J. T. Hupp, *J. Am. Chem. Soc.* **2023**, *145*, 4150.
[73] H. Xu, Y. Wu, L. Yang, Y. Rao, J. Wang, S. Peng, Q. Li, *Angew. Chem., Int. Ed. Engl.* **2023**, *62*, 202217864.
[74] Z. Lu, J. Duan, L. Du, Q. Liu, N. M. Schweitzer, J. T. Hupp, *J. Mater. Chem. A* **2022**, *10*, 6442.
[75] T. Y. Luo, S. Park, T. H. Chen, R. P. Prerna, X. Y. Li, J. I. Siepmann, S. Caratzoulas, Z. Y. Xia, M. Tsapatsis, *Angew. Chem., Int. Ed.* **2022**, *61*, 202209034.
[76] W. Gong, H. Xie, K. B. Idrees, F. A. Son, Z. Chen, F. Sha, Y. Liu, Y. Cui, O. K. Farha, *J. Am. Chem. Soc.* **2022**, *144*, 1826.
[77] H. X. Deng, C. J. Doonan, H. Furukawa, R. B. Ferreira, J. Towne, C. B. Knobler, B. Wang, O. M. Yaghi, *Science* **2010**, *327*, 846.
[78] Z. L. Zheng, N. Hanikel, H. Lyu, O. M. Yaghi, *J. Am. Chem. Soc.* **2022**, *144*, 22669.
[79] B. Tan, Y. Luo, X. Liang, S. Wang, X. Gao, Z. Zhang, Y. Fang, *Cryst. Growth Des.* **2020**, *20*, 6565.
[80] T. Stassin, S. Waitschat, N. Heidenreich, H. Reinsch, F. Pluschkell, D. Kravchenko, J. Marreiros, I. Stassen, J. van Dinter, R. Verbeke, M. Dickmann, W. Egger, I. Vankelecom, D. De Vos, R. Ameloot, N. Stock, *Chemistry* **2020**, *26*, 10841.
[81] J. X. Xu, T. X. Li, J. W. Chao, S. Wu, T. S. Yan, W. C. Li, B. Y. Cao, R. Z. Wang, *Angew. Chem., Int. Ed.* **2020**, *59*, 5202.
[82] K. J. Yang, Y. Shi, M. C. Wu, W. B. Wang, Y. Jin, R. Y. Li, M. W. Shahzad, K. C. Ng, P. Wang, *J. Mater. Chem. A* **2020**, *8*, 1887.
[83] L. Garzón-Tovar, J. Pérez-Carvajal, I. Imaz, D. Maspoch, *Adv. Funct. Mater.* **2017**, *27*, 1606424.
[84] G. Jajko, J. J. Gutiérrez-Sevillano, A. Sławek, M. Szufla, P. Kozyra, D. Matoga, W. Makowski, S. Calero, *Microporous Mesoporous Mater.* **2022**, *330*, 111555.
[85] I. V. Grenev, A. A. Shubin, M. V. Solovyeva, L. G. Gordeeva, *Phys. Chem. Chem. Phys.* **2021**, *23*, 21329.
[86] K. H. Cho, P. G. M. Mileo, J. S. Lee, U. H. Lee, J. Park, S. J. Cho, S. K. Chitale, G. Maurin, J. S. Chang, *ACS Appl. Mater. Interfaces* **2021**, *13*, 1723.
[87] J. Liu, R. Anderson, K. M. Schmalbach, T. R. Sheridan, Z. Wang, N. M. Schweitzer, A. Stein, N. A. Mara, D. Gomez-Gualdron, J. T. Hupp, *J. Mater. Chem. A* **2022**, *10*, 17307.
[88] Z. L. Zheng, H. L. Nguyen, N. Hanikel, K. K. Y. Li, Z. H. Zhou, T. Q. Ma, O. M. Yaghi, *Nat. Protoc.* **2022**, *18*, 136.
[89] F. Jeremias, D. Froehlich, C. Janiak, S. K. Henninger, *RSC Adv.* **2014**, *4*, 24073.
[90] D. D. Do, H. D. Do, *Carbon* **2000**, *38*, 767.
[91] L. H. Chen, W. K. Han, X. D. Yan, J. W. Zhang, Y. Q. Jiang, Z. G. Gu, *ChemSusChem* **2022**, *15*, 202201824.
[92] L. Stegbauer, M. W. Hahn, A. Jentys, G. Savasci, C. Ochsenfeld, J. A. Lercher, B. V. Lotsch, *Chem. Mater.* **2015**, *27*, 7874.
[93] S. Karak, S. Kandambeth, B. P. Biswal, H. S. Sasmal, S. Kumar, P. Pachfule, R. Banerjee, *J. Am. Chem. Soc.* **2017**, *139*, 1856.
[94] Y. Li, G. Wen, J. Li, Q. Li, H. Zhang, B. Tao, J. Zhang, *Chem. Commun. (Cambridge, U. K.)* **2022**, *58*, 11488.
[95] M. Rubio-Martinez, C. Avci-Camur, A. W. Thornton, I. Imaz, D. Maspoch, M. R. Hill, *Chem. Soc. Rev.* **2017**, *46*, 3453.
[96] Q. He, F. Zhan, H. Wang, W. Xu, H. Wang, L. Chen, *Mater. Today Sustainability* **2022**, *17*, 100104.
[97] P. A. Julien, C. Mottillo, T. Friščić, *Green Chem.* **2017**, *19*, 2729.
[98] K. Pobłocki, J. Drzeżdżon, B. Gawdzik, D. Jacewicz, *Green Chem.* **2022**, *24*, 9402.
[99] A. Permyakova, O. Skrylnyk, E. Courbon, M. Affram, S. Wang, U. H. Lee, A. H. Valekar, F. Nouar, G. Mouchaham, T. Devic, G. De Weireld, J.-S. Chang, N. Steunou, M. Frere, C. Serre, *ChemSusChem* **2017**, *10*, 1419.
[100] Z. Zheng, A. H. Alawadhi, O. M. Yaghi, *Mol. Front. J.* **2023**, https://doi.org/10.1142/S2529732523400011.
[101] D. Lenzen, P. Bendix, H. Reinsch, D. Froehlich, H. Kummer, M. Moellers, P. P. C. Huegenell, R. Glaeser, S. Henninger, N. Stock, *Adv. Mater.* **2018**, *30*, 1705869.
[102] S. Dai, F. Nouar, S. Zhang, A. Tissot, C. Serre, *Angew. Chem., Int. Ed.* **2021**, *60*, 4282.

[103] S. Dai, C. Simms, I. Dovgaliuk, G. Patriarche, A. Tissot, T. N. Parac-Vogt, C. Serre, *Chem. Mater.* **2021**, *33*, 7057.
[104] B. Karadeniz, A. J. Howarth, T. Stolar, T. Islamoglu, I. Dejanović, M. Tireli, M. C. Wasson, S.-Y. Moon, O. K. Farha, T. Friščić, K. Užarević, *ACS Sustainable Chem. Eng.* **2018**, *6*, 15841.
[105] D. Crawford, J. Casaban, R. Haydon, N. Giri, T. McNally, S. L. James, *Chem. Sci.* **2015**, *6*, 1645.
[106] M. Gaab, N. Trukhan, S. Maurer, R. Gummaraju, U. Müller, *Microporous Mesoporous Mater.* **2012**, *157*, 131.
[107] M. Rubio-Martinez, M. P. Batten, A. Polyzos, K.-C. Carey, J. I. Mardel, K.-S. Lim, M. R. Hill, *Sci. Rep.* **2014**, *4*, 5443.
[108] M. T. Kreutzer, F. Kapteijn, J. A. Moulijn, J. J. Heiszwolf, *Chem. Eng. Sci.* **2005**, *60*, 5895.
[109] M. Taddei, D. A. Steitz, J. A. van Bokhoven, M. Ranocchiari, *Chemistry* **2016**, *22*, 3245.
[110] L. Garzón-Tovar, M. Cano-Sarabia, A. Carné-Sánchez, C. Carbonell, I. Imaz, D. Maspoch, *React. Chem. Eng.* **2016**, *1*, 533.
[111] J. M. Pinheiro, S. Salústio, J. Rocha, A. A. Valente, C. M. Silva, *Renewable Sustainable Energy Rev.* **2020**, *119*, 109528.
[112] L. Calabrese, W. Mittelbach, L. Bonaccorsi, A. Freni, *Energies* **2022**, *15*, 5118.
[113] K. C. Ng, K. Thu, Y. Kim, A. Chakraborty, G. Amy, *Desalination* **2013**, *308*, 161.
[114] M. Ott, T. Wilde, H. Huber, presented at *2017 16th IEEE Intersociety Conference on Thermal and Thermomechanical Phenomena in Electronic Systems (ITherm)*, 30 May-2 June 2017, **2017**.
[115] C. Wu, L. Y. Chou, L. Long, X. Si, W. S. Lo, C. K. Tsung, T. Li, *ACS Appl. Mater. Interfaces* **2019**, *11*, 35820.
[116] X.-J. Xie, H. Zeng, M. Xie, W. Chen, G.-F. Hua, W. Lu, D. Li, *Chem. Eng. J.* **2022**, *427*, 132033.
[117] E. Elsayed, R. Al-Dadah, S. Mahmoud, A. Elsayed, P. A. Anderson, *Appl. Therm. Eng.* **2016**, *99*, 802.
[118] P. Youssef, S. Mahmoud, R. Al-Dadah, E. Elsayed, O. El-Samni, *Energy Procedia* **2017**, *142*, 1693.
[119] S. Sircar, J. R. Hufton, *Adsorption* **2000**, *6*, 137.
[120] B. Han, A. Chakraborty, *Microporous Mesoporous Mater.* **2019**, *288*, 109590.
[121] H. W. B. Teo, A. Chakraborty, *IOP Conf. Ser.: Mater. Sci. Eng.* **2017**, *272*, 012019.
[122] A. K. Cheetham, G. Kieslich, H. H. Yeung, *Acc. Chem. Res.* **2018**, *51*, 659.
[123] S. M. J. Rogge, M. Waroquier, V. Van Speybroeck, *Acc. Chem. Res.* **2018**, *51*, 138.
[124] M. Moayed Mohseni, M. Jouyandeh, S. Mohammad Sajadi, A. Hejna, S. Habibzadeh, A. Mohaddespour, N. Rabiee, H. Daneshgar, O. Akhavan, M. Asadnia, M. Rabiee, S. Ramakrishna, R. Luque, M. Reza Saeb, *Chem. Eng. J.* **2022**, *449*, 137700.
[125] B. Cui, C. O. Audu, Y. Liao, S. T. Nguyen, O. K. Farha, J. T. Hupp, M. Grayson, *ACS Appl. Mater. Interfaces* **2017**, *9*, 28139.
[126] B. L. Huang, Z. Ni, A. Millward, A. J. H. McGaughey, C. Uher, M. Kaviany, O. Yaghi, *Int. J. Heat Mass Transfer* **2007**, *50*, 405.
[127] J. Huang, X. Xia, X. Hu, S. Li, K. Liu, *Int. J. Heat Mass Transfer* **2019**, *138*, 11.
[128] M. Winterberg, E. Tsotsas, *Int. J. Therm. Sci.* **2000**, *39*, 556.
[129] Y. Yin, J. Shao, L. Zhang, Q. Cui, H. Wang, *J. Porous Mater.* **2021**, *28*, 1197.
[130] Z. Xu, Y. Yin, J. Shao, Y. Liu, L. Zhang, Q. Cui, H. Wang, *Energy* **2020**, *191*, 116302.
[131] H. Kim, S. R. Rao, E. A. Kapustin, L. Zhao, S. Yang, O. M. Yaghi, E. N. Wang, *Nat. Commun.* **2018**, *9*, 1191.
[132] H. A. Almassad, R. I. Abaza, L. Siwwan, B. Al-Maythalony, K. E. Cordova, *Nat. Commun.* **2022**, *13*, 4873.
[133] Y. Tao, J. Sun, Q. Wu, D. Zhu, H. Li, *Chem. Eng. J.* **2023**, *461*, 141864.
[134] Y. Ying, G. Yang, Y. Tao, Q. Wu, H. Li, *Adv. Sci.* **2023**, *10*, 2204840.
[135] Q. Li, Y. Ying, Y. Tao, H. Li, *Ind. Eng. Chem. Res.* **2022**, *61*, 1344.
[136] H. Shan, C. Li, Z. Chen, W. Ying, P. Poredos, Z. Ye, Q. Pan, J. Wang, R. Wang, *Nat. Commun.* **2022**, *13*, 5406.
[137] J. Y. Wang, R. Z. Wang, Y. D. Tu, L. W. Wang, *Energy* **2018**, *165*, 387.
[138] J. A. Shamim, W.-L. Hsu, K. Kitaoka, S. Paul, H. Daiguji, *Int. J. Heat Mass Transfer* **2018**, *116*, 1361.
[139] G. Angrisani, F. Minichiello, C. Roselli, M. Sasso, *Appl. Energy* **2012**, *92*, 563.
[140] H. Bahrehmand, M. Bahrami, *Int. J. Refrig.* **2019**, *100*, 368.
[141] S. Gökpinar, S.-J. Ernst, E. Hastürk, M. Möllers, I. El Aita, R. Wiedey, N. Tannert, S. Nießing, S. Abdpour, A. Schmitz, J. Quodbach, G. Füldner, S. K. Henninger, C. Janiak, *Ind. Eng. Chem. Res.* **2019**, *58*, 21493.
[142] P. Vivekh, M. Kumja, D. T. Bui, K. J. Chua, *Appl. Energy* **2018**, *229*, 778.
[143] L. Ge, T. Ge, R. Wang, *Renewable Sustainable Energy Rev.* **2022**, *157*, 112015.
[144] U. Betke, M. Klaus, J. G. Eggebrecht, M. Scheffler, A. Lieb, *Microporous Mesoporous Mater.* **2018**, *265*, 43.
[145] T. Yang, L. Ge, T. Ge, G. Zhan, R. Wang, *Adv. Funct. Mater.* **2022**, *32*, 2105267.
[146] Z. Chen, Z. Shao, Y. Tang, F. Deng, S. Du, R. Wang, *ACS Mater. Au* **2023**, *3*, 43.
[147] J.-G. Lee, K. J. Bae, O. K. Kwon, *Int. J. Refrig.* **2021**, *130*, 179.
[148] L. Chen, C. He, *Microporous Mesoporous Mater.* **2020**, *305*, 110378.
[149] F. Xu, Z. F. Bian, T. S. Ge, Y. J. Dai, C. H. Wang, S. Kawi, *Energy* **2019**, *177*, 211.
[150] Z. Liu, C. Cheng, J. Han, Z. Zhao, X. Qi, *Int. J. Refrig.* **2022**, *133*, 157.
[151] M. V. Solovyeva, L. G. Gordeeva, T. A. Krieger, Y. I. Aristov, *Energy Convers. Manage.* **2018**, *174*, 356.
[152] L. G. Gordeeva, M. V. Solovyeva, Y. I. Aristov, *Energy* **2016**, *100*, 18.
[153] M. V. Solovyeva, Y. I. Aristov, L. G. Gordeeva, *Appl. Therm. Eng.* **2017**, *116*, 541.
[154] M. M. Saleh, E. Elsayed, R. Al-Dadah, S. Mahmoud, *Therm. Sci. Eng. Prog.* **2022**, *28*, 101050.
[155] B. Panigrahi, H.-W. Wang, W.-J. Luo, Y.-C. Chou, J.-J. Chen, *Sci. Technol. Built Environ.* **2023**, *29*, 323.
[156] H. Kummer, F. Jeremias, A. Warlo, G. Fueldner, D. Frohlich, C. Janiak, R. Glaeser, S. K. Henninger, *Ind. Eng. Chem. Res.* **2017**, *56*, 8393.
[157] E. Gkaniatsou, C. Chen, F. S. Cui, X. Zhu, P. Sapin, F. Nouar, C. Boissière, C. N. Markides, J. Hensen, C. Serre, *Cell Rep. Phys. Sci.* **2022**, *3*, 100730.
[158] P. Bendix, G. Fueldner, M. Moellers, H. Kummer, L. Schnabel, S. Henninger, H.-M. Henning, *Appl. Therm. Eng.* **2017**, *124*, 83.
[159] M. Qin, P. Hou, Z. Wu, J. Wang, *Build. Environ.* **2020**, *169*, 106581.
[160] A. N. Aziz, S. Mahmoud, R. Al-Dadah, M. A. Ismail, M. K. A. Mesfer, *Appl. Therm. Eng.* **2022**, *215*, 118940.
[161] S. Z. Shahvari, J. D. Clark, *Appl. Energy* **2023**, *331*, 120421.
[162] T. Wilde, M. Ott, A. Auweter, I. Meijer, P. Ruch, M. Hilger, S. Kühnert, H. Huber, presented at *2017 33rd Thermal Measurement, Modeling & Management Symposium (SEMI-THERM)*, 13–17 March 2017, **2017**.
[163] X. She, L. Cong, B. Nie, G. Leng, H. Peng, Y. Chen, X. Zhang, T. Wen, H. Yang, Y. Luo, *Appl. Energy* **2018**, *232*, 157.
[164] S. A. Nada, H. F. Elattar, A. Fouda, *Int. J. Energy Res.* **2019**, *43*, 6812.
[165] M. Sultan, I. I. El-Sharkawy, T. Miyazaki, B. B. Saha, S. Koyama, *Renewable Sustainable Energy Rev.* **2015**, *46*, 16.
[166] N. Enteria, H. Yoshino, A. Satake, A. Mochida, R. Takaki, R. Yoshie, S. Baba, *Appl. Energy* **2010**, *87*, 478.
[167] T. Miyazaki, I. Nikai, A. Akisawa, *Int. J. Energy Clean Environ.* **2011**, *12*, 341.
[168] D. Pandelidis, S. Anisimov, W. M. Worek, P. Drąg, *Energy Build.* **2017**, *140*, 154.

[169] S. Abdullah, M. N. B. Zubir, M. R. Bin, K. M. S. N Muhamad, H. F. Oztop, M. S. Alam, K. Shaikh, *Energy Build.* **2023**, *283*.
[170] D. B. Jani, M. Mishra, P. K. Sahoo, *Renewable Sustainable Energy Rev.* **2016**, *60*, 1451.
[171] M. H. Mahmood, M. Sultan, T. Miyazaki, S. Koyama, V. S. Maisotsenko, *Renewable Sustainable Energy Rev.* **2016**, *66*, 537.
[172] M. F. Habib, M. Ali, N. A. Sheikh, A. W. Badar, S. Mehmood, *J. Build. Eng.* **2020**, *30*, 101279.
[173] T. Pandey, P. K. S. Tejes, B. K. Naik, *Desalination* **2022**, *537*, 115843.
[174] S. Anisimov, D. Pandelidis, A. Jedlikowski, V. Polushkin, *Energy* **2014**, *76*, 593.
[175] S. Z. Shahvari, V. A. Kalkhorani, J. D. Clark, *Int. J. Refrig.* **2022**, *140*, 186.
[176] S. Ashraf, M. Sultan, G. Hussain, S. Noor, H. Ashraf, T. Miyazaki, R. Shamshiri, R. Kanwal, M. Mahmood, M. Taseer, *Fresenius Environ. Bull.* **2021**, *30*, 7375.
[177] R. V. Wahlgren, *Water Res.* **2001**, *35*, 1.
[178] A. K. Rao, A. J. Fix, Y. C. Yang, D. M. Warsinger, *Energy Environ. Sci.* **2022**, *15*, 4025.
[179] M. N. Dods, S. C. Weston, J. R. Long, *Adv. Mater.* **2022**, *34*, 2204277.
[180] Y. Sun, A. Spiess, C. Jansen, A. Nuhnen, S. Goekpinar, R. Wiedey, S.-J. Ernst, C. Janiak, *J. Mater. Chem. A* **2020**, *8*, 13364.
[181] N. Hanikel, M. S. Prevot, O. M. Yaghi, *Nat. Nanotechnol.* **2020**, *15*, 348.
[182] N. Hanikel, M. S. Prevot, F. Fathieh, E. A. Kapustin, H. Lyu, H. Wang, N. J. Diercks, T. G. Glover, O. M. Yaghi, *ACS Cent. Sci.* **2019**, *5*, 1699.
[183] H. Kim, S. Yang, S. R. Rao, S. Narayanan, E. A. Kapustin, H. Furukawa, A. S. Umans, O. M. Yaghi, E. N. Wang, *Science* **2017**, *356*, 430.
[184] Y. H. Feng, R. Z. Wang, T. S. Ge, *Adv. Sci.* **2022**, *9*, 2204508.
[185] T. X. Li, M. Q. Wu, J. X. Xu, R. X. Du, T. S. Yan, P. F. Wang, Z. Y. Bai, R. Z. Wang, S. Q. Wang, *Nat. Commun.* **2022**, *13*, 6771.
[186] T. H. Smith, D. S. Kuo, E. A. Kapustin, B. Marchon, F. S. Maniar *Patent WO 2021/162894 A1*, **2021**.
[187] E. Switzer, C. Friesen, H. Lorzel, *Patent WO 2016/081863 A1*, **2016**.
[188] Source global, Introducing the hydropanel, https://www.source.co/ (accessed: June 2023).
[189] A. LaPotin, Y. Zhong, L. A. Zhang, L. Zhao, A. Leroy, H. S. R. Rao, E. N. Wang, H. Kim, *Joule* **2021**, *5*, 166.
[190] A. Terzis, A. Ramachandran, K. C. Wang, M. Asheghi, K. E. Goodson, J. G. Santiago, *Cell Rep. Phys. Sci.* **2020**, *1*, 14.
[191] H. Sharon, K. S. Reddy, *Renewable Sustainable Energy Rev.* **2015**, *41*, 1080.
[192] C. Li, Y. Goswami, E. Stefanakos, *Renewable Sustainable Energy Rev.* **2013**, *19*, 136.
[193] K. C. Ng, K. Thu, B. B. Saha, A. Chakraborty, *Int. J. Refrig.* **2012**, *35*, 685.
[194] P. G. Youssef, H. Dakkama, S. M. Mahmoud, R. K. Al-Dadah, *Desalination* **2017**, *404*, 192.
[195] E. Elsayed, R. Al-Dadah, S. Mahmoud, P. A. Anderson, A. Elsayed, P. G. Youssef, *Desalination* **2017**, *406*, 25.
[196] Y. C. Wang, X. X. Xia, D. C. Shen, Z. K. Tu, X. B. Luo, S. Li, *Appl. Therm. Eng.* **2022**, *215*.
[197] E. Elsayed, R. Al-Dadah, S. Mahmoud, P. Anderson, A. Elsayed, *Desalination* **2020**, *475*, 114170.
[198] B. Han, A. Chakraborty, *Energy Convers. Manage.* **2020**, *213*, 112825.
[199] M. Chorazewski, P. Zajdel, T. Feng, D. Luo, A. R. Lowe, C. M. Brown, J. B. Leao, M. Li, M. Bleuel, G. Jensen, D. Li, A. Faik, Y. Grosu, *ACS Nano* **2021**, *15*, 9048.
[200] B.-X. Han, Y.-F. Jiang, X.-R. Sun, Z.-F. Li, G. Li, *Coord. Chem. Rev.* **2021**, *432*, 213754.
[201] Z. Guo, Y. Zhang, J. Liu, B. Han, G. Li, *New J. Chem.* **2021**, *45*, 16971.
[202] H. Gao, Y.-B. He, J.-J. Hou, X.-M. Zhang, *ACS Appl. Mater. Interfaces* **2021**, *13*, 38289.
[203] Q. Yang, Y. Wang, Y. Shang, J. Du, J. Yin, D. Liu, Z. Kang, R. Wang, D. Sun, J. Jiang, *Cryst. Growth Des.* **2020**, *20*, 3456.
[204] Z. Zhang, Q. Han, S. Zhang, X. Guo, H. Huang, F. Yang, C. Zhong, *ACS Sustainable Chem. Eng.* **2022**, *10*, 11867.
[205] L. J. Small, M. E. Schindelholz, T. M. Nenoff, *Ind. Eng. Chem. Res.* **2021**, *60*, 7998.
[206] F. Tan, L. Zha, Q. Zhou, *Adv. Mater.* **2022**, *34*, 2201470.
[207] J. Xu, J. Chao, T. Li, T. Yan, S. Wu, M. Wu, B. Zhao, R. Wang, *ACS Cent. Sci.* **2020**, *6*, 1542.
[208] E. Gkaniatsou, B. Meng, F. Cui, R. Loonen, F. Nouar, C. Serre, J. Hensen, *Nano Energy* **2021**, *87*, 106224.
[209] Bosch, PerfectDry Dishwasher based on Zeolith, https://www.bosch-home.com/mt/bosch-innovations/perfectdry (accessed: April 2023).
[210] Siemens-BSH, Dishwasher with Zeolith drying technology, https://www.siemens-home.bsh-group.com/nl/inspiratie/highlights/zeolith (accessed: 06 March 2023).
[211] A. Hauer, F. Fischer, *Chem. Ing. Tech.* **2011**, *83*, 61.
[212] G. Santori, A. Frazzica, A. Freni, M. Galieni, L. Bonaccorsi, F. Polonara, G. Restuccia, *Energy* **2013**, *50*, 170.
[213] M. Erdogan, S. Graf, U. Bau, F. Lanzerath, A. Bardow, *Appl. Therm. Eng.* **2017**, *125*, 1075.
[214] M. Erdogan, U. Bau, A. Bardow, *Appl. Therm. Eng.* **2019**, *160*, 113942.
[215] J. Cranston, A. Askalany, G. Santori, *Energy* **2019**, *183*, 683.
[216] M. I. Severino, E. Gkaniatsou, F. Nouar, M. L. Pinto, C. Serre, *Faraday Discuss.* **2021**, *231*, 326.
[217] H. Luo, F. Cheng, L. Huelsenbeck, N. Smith, *J. Environ. Chem. Eng.* **2021**, *9*, 105159.
[218] D. DeSantis, J. A. Mason, B. D. James, C. Houchins, J. R. Long, M. Veenstra, *Energy Fuels* **2017**, *31*, 2024.
[219] Avantium, PEF bottles – a sustainable packaging material, https://www.avantium.com/wp-content/uploads/2022/02/20220221-PEF-bottles-%E2%80%93-a-sustainable-packaging-material-ISO-certified-LCA.pdf (accessed: April 2023).
[220] S. Graf, S. Eibel, F. Lanzerath, A. Bardow, *Energy Technol.* **2020**, *8*, 1901130.
[221] U. Bau, N. Baumgartner, J. Seiler, F. Lanzerath, C. Kirches, A. Bardow, *Appl. Therm. Eng.* **2019**, *149*, 1503.
[222] B. Dawoud, *J. Chem. Eng. Jpn.* **2007**, *40*, 1298.
[223] R. Li, Y. Shi, M. Wu, S. Hong, P. Wang, *Nano Energy* **2020**, *67*, 104255.
[224] G. Yilmaz, F. L. Meng, W. Lu, J. Abed, C. K. N. Peh, M. Gao, E. H. Sargent, G. W. Ho, *Sci. Adv.* **2020**, *6*, eabc8605.
[225] F. Luo, X. Liang, W. Chen, S. Wang, X. Gao, Z. Zhang, Y. Fang, *Chem. Eng. J.* **2022**, *450*, 138241.
[226] S. Graf, F. Lanzerath, A. Bardow, *Appl. Therm. Eng.* **2017**, *126*, 630.
[227] M. Bilal, M. Sultan, T. Morosuk, W. Den, U. Sajjad, M. M. A. Aslam, M. W. Shahzad, M. Farooq, *Int. Commun. Heat Mass Transfer* **2022**, *133*, 105961.
[228] W. Li, X. Xia, S. Li, *J. Mater. Chem. A* **2019**, *7*, 25010.
[229] A. J. Rieth, A. M. Wright, S. Rao, H. Kim, A. D. LaPotin, E. N. Wang, M. Dinca, *J. Am. Chem. Soc.* **2018**, *140*, 17591.
[230] M. Engelpracht, J. Driesel, O. Niessen, M. Henninger, J. Seiler, A. Bardow, *Energy Technol.* **2022**, *10*, 2200251.
[231] E. Commission, Annex G. Technology Readiness Levels (TRL), https://ec.europa.eu/research//h2020-wp1415-annex-g-trl_en.pdf (accessed: June 2023).
[232] R. Al-Dadah, S. Mahmoud, E. Elsayed, P. Youssef, F. Al-Mousawi, *Energy* **2020**, *190*, 116356.
[233] L. Giordano, J. Gubis, G. Bierman, F. Kapteijn, *J. Membr. Sci.* **2019**, *575*, 229.

[234] N. Baumgartner, S. Deutz, C. Reinert, N. Nolzen, L. E. Kuepper, M. Hennen, D. E. Hollermann, A. Bardow, *Front. Energy Res.* **2021**, *9*, 621502.
[235] U. Eicker, U. Schürger, M. Köhler, T. Ge, Y. Dai, H. Li, R. Wang, *Appl. Therm. Eng.* **2012**, *42*, 71.
[236] A. M. Baniyounes, M. G. Rasul, M. M. K. Khan, *Energy Build.* **2013**, *62*, 78.
[237] N. Enteria, H. Yoshino, A. Mochida, R. Takaki, A. Satake, R. Yoshie, T. Mitamura, S. Baba, *Sol. Energy* **2009**, *83*, 1300.
[238] C. McCague, W. Huttema, A. Fradin, M. Bahrami, *Appl. Therm. Eng.* **2020**, *173*, 115219.
[239] W. T. Xu, O. M. Yaghi, *ACS Cent. Sci.* **2020**, *6*, 1348.

Bo Zhang is a Ph.D. candidate under the supervision of Prof. Xinlei Liu at the School of Chemical Engineering and Technology at Tianjin University. He received his Bachelor's Degree in Engineering in 2020 at China University of Petroleum (East China). He is interested in gas–liquid flow and mass transfer and MOF membranes for isomer separation.

Zerui Zhu is a Master's degree candidate under the supervision of Prof. Xuerui Wang at College of Chemical Engineering at Nanjing Tech University. He received his Bachelor's Degree in Engineering in 2022 at Changzhou University. He is interested in microporous membranes and (noble) gas separation in energy- and environment-related fields.

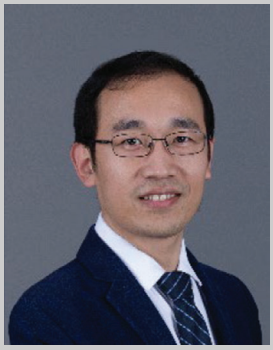

Xuerui Wang is a professor at College of Chemical Engineering at Nanjing Tech University. He received his Ph.D. in 2014 at Nanjing Tech University and held postdoc positions at National University of Singapore (2015–2017) and Delft University of Technology (2017–2019). He is interested in microporous membranes and (noble) gas separation in energy- and environment-related fields.

Xinlei Liu is a professor at School of Chemical Engineering and Technology at Tianjin University. He received his Ph.D. in 2013 at the Dalian Institute of Chemical Physics and held postdoc positions at Imperial College London (2013–2016) and Delft University of Technology (2016–2019). He is interested in membranes and porous framework chemistry for energy and environmental science.

Freek Kapteijn is an emeritus professor in Catalysis Engineering from the Delft University of Technology. His scientific interest covers the application of heterogeneous catalysts and porous materials for efficient utilization of energy and feedstock. Specific research topics include the synthesis, characterization, and application of structured systems (metal-organic frameworks, zeolites, monoliths, catalytic membranes) in multiphase and multifunctional conversion processes, adsorption and diffusion in zeolites, MOFs and their membranes, and transient kinetics. Received in 2017 the prestigious Golden Hoogewerff medal for his Catalysis Engineering oeuvre and the IChemE Andrew medal for the same in 2018. He is still associated with activities at TUDelft.